NASA Contractor Report 4007

A Full Potential Flow Analysis With Realistic Wake Influence for Helicopter Rotor Airload Prediction

T. Alan Egolf and S. Patrick Sparks
United Technologies Research Center
East Hartford, Connecticut

Prepared for
Ames Research Center
under Contract NAS2-11150

National Aeronautics
and Space Administration

Scientific and Technical
Information Branch

1987

CONTENTS

PREFACE

This investigation was sponsored and administered by the National Aeronautics and Space Administration Ames Research Center, Moffett Field, California, under Contract NAS2-11150. The NASA Technical Monitor for this contract was Michael Tauber. The Principal Investigator was T. Alan Egolf, Senior Research Engineer, United Technologies Research Center (UTRC). The Co-investigator was S. Patrick Sparks, Assistant Research Engineer, UTRC. Consulting support during the initial formulation activity was provided by Joseph M. Verdon, Principle Scientist, UTRC. The Program Manager was Anton J. Landgrebe, Manager, Aeromechanics Research, UTRC.

SUMMARY

A three-dimensional, quasi-steady, full potential flow solver was adapted to include realistic wake influence for the aerodynamic analysis of helicopter rotors. The method is based on a finite difference solution of the full potential equation, using an inner and outer domain procedure to accommodate wake effects. The nonlinear flow is computed in the inner domain region, relative to the blade, using a finite difference solution method. The wake is modeled by a vortex lattice using prescribed geometry techniques to allow for the inclusion of realistic rotor wakes. The key feature of the analysis is that vortices contained within the finite difference mesh (inner domain) are treated with a vortex embedding technique while the influence of the remaining portion of the wake (in the outer domain) is impressed as a boundary condition on the outer surface of the finite difference mesh. The solution procedure couples the wake influence with the inner domain solution in a consistent and efficient solution process. The method, termed ROT22/WAKE, has been applied to both hover and forward flight conditions. Correlation with subsonic and transonic hover airload data is shown which demonstrates the merits of the approach.

LIST OF SYMBOLS

a	Local speed of sound.
A	A grid stretching parameter.
B	Denotes the finite difference (inner) domain boundary. Also a grid stretching parameter.
c	Blade section chord length.
C	The grid stretching parameter used to make the physical mesh finite in extent.
C_l	Section lift coefficient, reference to the local blade chord and a dynamic pressure based on the local freestream velocity $\vec{V}_\infty$.
C_p	Pressure coefficient, referenced to a dynamic pressure based on the local freestream velocity, $\vec{V}_\infty$.
C_T	Rotor thrust coefficient.
i, j, k	Cartesian unit vectors, blade-fixed frame, corresponding to x, y, and z.
L( )	Linear differential operator; e.g., $\vec{\nabla}\cdot(\ )$
M	Mach number.
n	Unit normal at blade surface; positive pointing into the fluid.
N( )	Nonlinear differential operator; e.g., the full potential equation operator.
P	CPU cost parameter.
r	Position vector, relative to the origin of the blade-fixed coordinate system, x, y, z.
R	Rotor tip radius.
S	Path of integration on the outer boundary surface of the inner domain.
u	Total velocity component, x-direction, blade-fixed system, in the inner domain.

$\vec{U}_\infty$ The blade-relative onset velocity, due only to the translational speed of the aircraft.

v Total velocity component, y-direction, blade-fixed system, in the inner domain.

$\vec{V}_\infty$ The blade-relative freestream velocity, composed of the onset velocity $\vec{U}_\infty$ and the rotational components $\vec{\omega} \times \vec{r}$.

$\vec{V}$ Total velocity in the inner domain, blade-fixed system.

w Total velocity component, z-direction, blade-fixed system, in the inner domain.

x Blade-fixed coordinate in the chordwise direction, in the tip-path-plane.

$\bar{X}$ Computational coordinate; $0 < \bar{X} < 1$, typically

$\bar{X}_m$ Denotes the extent of the unstretched grid in computational space.

y Blade-fixed coordinate in the direction normal to the tip-path-plane.

z Blade-fixed coordinate in the spanwise direction, in the tip-path-plane.

Greek

α Attitude of the rotor tip-path-plane relative to the flight direction; defined positive for tilt-back.

μ Advance ratio, defined as the flight speed divided by the rotational tip speed.

θ Total blade pitch at the 0.75R radial station.

$\vec{\nabla}$ Gradient operator, del.

$\vec{\nabla}\cdot$ Divergence operator.

ϕ Reduced velocity potential.

ψ Azimuth position of the blade.

$\vec{\omega}$ Angular velocity vector of the rotor

Superscripts

'	Prime indicates velocities in the outer domain.
*	Indicates inertial reference frame.

Subscripts

1	Indicates velocities associated with the embedded portion of the wake only.
2	Indicates velocities associated with all of the wake except the embedded portion; that is, the wake external to the inner domain.
TIP	Tip Mach number based on rotational speed only.

Special operator

[[ ]]	Denotes the difference in a quantity across a surface (lower minus upper).

INTRODUCTION

The flow around a helicopter rotor blade is generally characterized by unsteady, non-uniform inflow with close blade/vortex passages combined with operating conditions which can include transonic flow. The complicated three-dimensional rotor wake has a dominant influence on the blade loading in both hover and forward flight (e.g., refs. 1-17). Transonic conditions are common on the advancing blades in forward flight, providing an extreme design challenge for the aerodynamicist and acoustician. Thus far, the analysis of the complete rotor problem has been largely intractable without relying on many compromising assumptions.

Any complete analysis of the helicopter rotor and wake must account for three distinct yet coupled phenomena:

1. The nonlinear compressible flow near the blade
2. The highly complex, but essentially low speed wake flow
3. Close blade/vortex interaction

Analyses for each of these aspects of the problem already exist, though not in a rigorously coupled form. Typically, modeling of the complete rotor and wake has been accomplished with lifting-line and lifting surface methods using vortex or doublet singularities to represent the wake. The geometry of the wake is either prescribed or computed. This approach gives rapid and reasonably accurate predictions of airloads (refs. 1-17) but only approximates the compressibility effects on the blade and cannot give the details of the surface flow. Close blade/vortex interactions in transonic flow have been studied with finite difference methods in two-dimensional unsteady flow (e.g., ref. 18), in three-dimensional steady flow, fixed-wing, (ref. 19), and for the helicopter rotor (ref. 20-21). These typically have been limited to simple interactions, involving only one or two infinite length vortices. They have not included complex, multiple interactions. Also, these analyses lack the global influence of the whole wake.

A three-dimensional unsteady transonic small disturbance solution has been developed by Caradonna, reference 22, which includes the global wake influence. That method is termed an integral-differential hybrid scheme and couples a vortex-lattice type wake model with a finite difference flow solver. The wake influence is accounted for by adjusting the local blade geometric angle-of-attack by an induced angle obtained from the wake model. The technique is very efficient and has shown agreement with experiment, but the rigorous validity of adjusting the blade incidence is questionable for close blade/vortex interactions. A recent effort to incorporate the complete wake influence using a full potential method was reported in reference 23. This approach used the same angle-of-attack adjustment method as reference 22. Other recent efforts to solve the rotor and wake problem have used conservative full potential (refs. 24-25) and Euler methods (refs. 26-27).

The present report describes the development of a quasi-steady full potential aerodynamic analysis for helicopter rotors that computes transonic flow on the blade, includes the complex distorted wake influence, and more rigorously treats close blade/vortex interactions. The full potential method of Arieli and Tauber (ref. 28) was adapted and expanded to include realistic wake influence. Viscous effects are not included. The analysis consists of a finite difference full potential scheme for the near blade flow and a prescribed vortex lattice wake model. The finite difference region is termed the inner domain. The flow outside this region is in the outer domain and is solved using the vortex lattice method. Coupling between the inner and outer domains is provided through the boundary values on the outer surface of the inner domain and also by proper accounting of that portion of the vortex wake that passes into the inner domain. Because most of complex wake geometry of the rotor blades is outside of the inner domain, an efficient solution process results. A description of the method follows.

TECHNICAL APPROACH

The current method of computing the rotor and wake flow was developed by combining two distinct solution techniques: the vortex lattice/lifting-line method and the finite difference method applied to the full potential equation. Rotor and wake calculations have been performed extensively with the vortex lattice/lifting-line methods for many years. These have been shown to give reasonable predictions of performance, but are unable to capture the details of the flow, and rely on empirical data to simulate transonic effects. Finite difference solutions have been applied to the rotor problem and are capable of computing nonlinear compressible flows with shocks.

The quasi-steady full potential finite difference flow analysis ROT22, developed by Arieli and Tauber (ref. 28), was chosen as the basis of the current development. This program is the rotary wing extension of Jameson's FLO22 analysis (ref. 29) for fixed wing calculations of transonic flow. The method is based on the discretization of the full potential equation in quasi-linear form, using the Jameson rotated differencing scheme in supersonic regions. This formulation is called 'non-conservative', meaning that the difference equation does not take the form of a conservation law and hence, conservation of mass across shock waves is not enforced.

A vortex lattice model was developed to model the rotor wake. This model is constructed using straight, constant strength Biot-Savart vortex segments in the form of vortex boxes. The wake geometry is prescribed, typically as a hover or forward flight generalization (refs. 6, 9, and 14) or as classical skewed helical surfaces. In principle, any means of defining the wake geometry can be accommodated, including free-wake methods.

Coupling of the vortex lattice wake with the full potential (inner domain) solution is accomplished by an inner and outer solution matching procedure which is discussed next.

Discussion of the Procedure for Matching an Inner and Outer Solution

Consider a three-dimensional flow past a finite lifting body. This body generates a wake represented by a trailing vortex sheet; i.e., a material surface. This surface is not necessarily planar and its position in space is not known a priori, but can be defined approximately based on empirical or free-wake considerations. There is a mutual influence between the body and its wake. Figure 1 illustrates the inner and outer domain concept for a two dimensional section of three-dimensional space.

In continuous regions of the inviscid transonic flow, the nonlinear isentropic flow equation, $N[\vec{V}] = 0$, is assumed to apply. Let $\vec{V}$ represent a solution of this equation valid in a region near the body (i.e. an inner domain). This inner domain contains the body and is bounded by the surface, B, which is placed at some prescribed distance from the body. If the flow beyond this boundary, i.e. in the outer domain, is subsonic then the velocity in this region can be approximated as the solution of a linear differential equation, $L[\vec{V}'] = 0$. In some applications, the flow in the outer domain can be regarded as incompressible and hence $L[\vec{V}'] = \vec{\nabla} \cdot (\vec{V}') = 0$ will apply in the outer flow domain. The inner and outer velocities must match at the prescribed boundary, B.

To successfully apply this concept, it is necessary to determine an analytic solution to $L[\vec{V}'] = 0$ which has the proper behavior away from the body and can be matched to an inner numerical solution of the full potential equation at the boundary B. This solution should be expressible in terms of unknown constant coefficients and recognize the influence of the body and its wake. If such a solution can be found, then the matching conditions on B can be used to specify the unknown coefficients of the outer domain solution in terms of the inner domain solution.

A linear solution in the outer domain is difficult to determine for three dimensional compressible flow; in fact, for rotary wings no simple model exists. As an approximation, a solution as determined from an incompressible lifting-line/vortex lattice wake model is used in the outer region. This solution will be somewhat inaccurate in the far field since the compressible solution differs from the incompressible solution (ref. 30). Such an approximation is desirable because it results in a low cost solution for the outer domain and relies on established methods. The effect of this modeling assumption is discussed later in the report.

To complete the general discussion of the inner and outer domain solution, it is necessary to deal with that part of the wake which passes into the inner domain. This is termed the embedded part of the wake and is indicated schematically in figure 1. While most of the wake influence can be accounted for through the domain matching procedure, those vortex elements which are inside the finite difference domain are included by vortex embedding. The specific equations and solution method are now developed below.

Inner/Outer Domain Formulation for the Rotary Wing Problem

Governing Equation. - The theoretical development of the quasi-steady full potential solution of helicopter rotor flows can be found in Arieli and Tauber, reference 28. There the steady fixed wing formulation was extended to

the rotor problem by the appropriate transformation to the rotating frame. The coordinate system is shown in figure 2, where the blade fixed axes are denoted by x, y, and z such that x is the chordwise direction, y vertical, and z spanwise; and the inertial system is (x*, y*, z*). (Note: ref. 28 presents a left-handed coordinate system. A right-handed system is used here. As a result the direction of rotation is non-standard, but it is consistent with the chosen orientation of the axes.) Following reference 28 the governing equation is, in the blade-fixed reference frame,

$$
\begin{aligned}
&(a^2 - u^2)\, u_x + (a^2 - v^2)\, v_y + (a^2 - w^2)\, w_z + \\
&- uv\,(u_y + v_x) - uw\,(u_z + w_x) - vw\,(v_z + w_y) + \\
&+ \omega^2\,[x\,(u - \omega z) + z\,(w + \omega x)] + \omega\mu\cos\alpha[\omega(x\sin\psi + z\cos\psi) \\
&- 2u\cos\psi + 2w\sin\psi] = 0
\end{aligned}
\tag{1}
$$

where ω is the angular velocity of the rotor, and u, v, and w are the cartesian components of $\vec{V}$, the total velocity in the blade-fixed frame. The local sound speed, a, is

$$
a^2 = a_\infty^2 + \frac{\gamma - 1}{2}\,(\vec{V}_\infty^2 - \vec{V}^2) \tag{2}
$$

where a_∞ is the speed of sound in the undisturbed air, and the blade relative freestream velocity is

$$
\vec{V}_\infty = \omega z\vec{i} - \omega x\vec{k} + \vec{U}_\infty \tag{3}
$$

The onset velocity, $\vec{U}_\infty$, is given by

$$
\vec{U}_\infty = \mu[\cos\alpha\,\sin\psi\,\vec{i} + \sin\alpha\,\vec{j} + \cos\alpha\,\cos\psi\,\vec{k}] \tag{4}
$$

where μ is the rotor advance ratio. The angle of attack, α is the incidence made by the rotor tip-path plane relative to the flight direction, such that positive α is for aftward tilt of the rotor disk (nose up). Lengths are normalized by the blade radius, R, and velocity is normalized by blade rotational tip speed, ωR. The derivation of equations (1) and (2) is based on the conservation of mass and energy under the assumptions of isentropic flow and irrotationality.

For the inner/outer domain formulation it is necessary to recast these expressions to allow the presence of the embedded vortices in the solution domain. These embedded vortices are modeled using the Biot-Savart Law. It is to be noted that not all Biot-Savart vortices are irrotational (e.g., a finite length vortex segment, or a vortex with a core model). In the present work, however, the method is developed specifically for irrotational wake elements, though a core is used to avoid numerical difficulties associated with the singular points.

Vortex Embedding. - In the discussion of the vortex embedding technique, reference is made to figure 3 (a, b, and c) where the inner and outer domains are pictured as typical for the current analysis (one blade is shown for simplicity). The decomposition into embedded and outer domain portions is given in figures 3b and 3c. Each figure gives top and side views of the blade, wake, and inner domain.

A scheme was developed to include the effects of those vortex wake elements that are inside the inner domain, as depicted in figure 3b. The procedure is based on that of Steinhoff for including the effects of vortices in potential calculations in reference 19. It has also been used by McCroskey in reference 18 where it is called the prescribed-disturbance method.

In the present method, the velocity field induced by the wake is decomposed into two parts, $\vec{V}_1$ and $\vec{V}_2$. All wake elements inside the finite difference domain are considered to have influence $\vec{V}_1$ and all those outside the domain have influence $\vec{V}_2$ (fig. 3c). Note that the portion of the wake contained "inside" the branch cut is not an embedded wake surface. Any element partly inside contributes to $\vec{V}_1$. Hence, the solution inside the finite difference domain is defined to be rotating frame freestream components plus the potential flow, plus the embedded field:

$$\vec{V} = \vec{V}_\infty + \vec{\nabla}\phi + \vec{V}_1 \tag{5}$$

where $\vec{\nabla}\phi$ is solved for as discussed in the next section. In this form, the potential function is termed a reduced potential (ref. 28) since it has been separated from the onset velocity $\vec{U}_\infty$.

Equation (5) does not imply linear superposition. Rather, this combined velocity is substituted into the flow equations, equations (1) and (2). Thus equation (1) can be rewritten as an equation for ϕ with an inhomogeneous term on the right hand side:

$$
\begin{aligned}
&(a^2 - u^2)\,\phi_{xx} + (a^2 - v^2)\,\phi_{yy} + (a^2 - w^2)\,\phi_{zz} + \\
&- 2\,uv\,\phi_{xy} - 2\,uw\phi_{xz} - 2\,vw\,\phi_{yz} \\
&+ \omega^2\,(x\phi_x + z\phi_z) - 2\omega\mu\cos\alpha(\phi_x\cos\psi - \phi_z\sin\psi) \\
&= (u^2 u_{1x} + v^2\,v_{1y} + w^2 w_{1z}) + 2(uv\,u_{1y} + uwu_{1z} + vwv_{1z}) \\
&- \omega^2(xu_1 + zw_1) + 2\omega\mu\cos\alpha(u_1\cos\psi - w_1\sin\psi)
\end{aligned}
\tag{6}
$$

and equation (2) remains the same, but with the definition of $\vec{V}$ as given in equation (5).

The flow in the outer domain is defined by the linear superposition of all the wake elements,

$$\vec{V}' = \vec{V}_\infty + \vec{V}_1 + \vec{V}_2 \quad . \tag{7}$$

Thus, with prescribed wake geometry and strength, the $\vec{V}_1$ and $\vec{V}_2$ velocity fields can be computed by the vortex lattice method and used in equation (6) for the solution of the potential. Recall that the rotor wake geometry is a function of blade geometry, operating condition, and rotor thrust (refs. 4, 6, and 14). Since the influence of the wake is also a function of the wake geometry and the blade circulation distribution, it is possible to construct an iteration scheme: the solution of the potential equation gives a blade loading and hence thrust and circulation, from which new wake geometry and strengths are obtained. The details of the procedure will follow in a later section.

Outer Boundary Condition. - To establish the outer boundary condition for the full potential solution, the velocity fields of the inner and outer domains are required to match on the boundary of the finite difference mesh:

$$[\vec{V}'] = [\vec{V}] \tag{8}$$

which gives

$$[\vec{\nabla}(\phi)] = [\vec{V}_2]. \tag{9}$$

Hence, only those elements associated with $\vec{V}_2$, as in figure 3c, contribute to the outer boundary condition. (Note that while the lifting line and wake just downstream of the blade appear to be inside the inner domain, they are actually external to it, since there is a branch cut from the airfoil trailing edge.) Equation (9) can be integrated to provide boundary values on the outer surface of the finite difference domain through the relation

$$\phi = \int_B \vec{V}_2 \cdot d\vec{S} \tag{10}$$

where $\vec{S}$ represents a path on the outer surface, B, of the domain. Clearly $\vec{V}_2$ must be irrotational, else no potential could exist for it. It is evident that some types and/or combinations of vortex elements can introduce vorticity, thereby violating this requirement. There is the same restriction on $\vec{V}_1$. It is obtained here from the Biot-Savart Law and as such is a solution of the incompressible continuity equation (as reflected by eq. (6)), but this is no guarantee of irrotational flow. Therefore the types of wake elements are restricted to those which individually produce potential fields. The vortex box was used in this investigation because it is a simple element that satisfies the irrotationality condition and it is equivalent to a conventional lattice method.

Blade Surface Boundary Condition. - To enforce the flow tangency condition on the blade surface, the velocity at the surface must satisfy

$$\vec{V} \cdot \vec{n} = 0. \tag{11}$$

As in the other equations presented, $\vec{V}$ is defined by equation (5).

Wake Boundary Condition. - The final conditions required to give a solution to the full potential equation are the Kutta condition at the trailing edge of the blade and a wake boundary condition. The Kutta condition is set by enforcing that the flow leave the trailing edge at the mean trailing edge angle. This is implemented in practice by making the branch cut of the finite difference mesh follow this mean angle as it leaves the trailing edge. The wake condition is established by enforcing an approximate convection relation for the trailing edge circulation,

$$[[\phi]]_{TE} = [[\phi]]_{WAKE} \tag{12}$$

This is used in the finite difference formulation to set the jump in potential across the wake at each grid point associated with the wake.

Finite Difference Solution of the Full Potential Equation

The governing equation, equation (6) (and associated definitions equations (2), (3), (4), and (5)), is solved with the boundary conditions, equations (10), (11), and (12), by means of a finite difference technique that uses the Jameson rotated difference scheme and is described in reference 29. The numerical grid used is the sheared parabolic mesh used in FLO22, reference 29, and ROT22, reference 28.

Finite Inner Domain. - The finite difference mesh employed in ROT22/WAKE is constructed on a parabolic coordinate system. Node point locations are obtained in their Cartesian values through the parabolic transformation with shearing, translational, and rotational transformations added to give the body shape. It is then possible to solve the difference equations on a transformed mesh which is rectangular. The basic parabolic transformation is augmented by a stretching function which renders the computational domain finite, regardless of the size of the physical domain. Originally, this grid was designed to extend to infinity (in physical space) thereby allowing the specification of zero as the condition on the outer boundary. The stretching relation has been altered to permit the physical inner domain to be finite. The stretching is demonstrated by the following example for one coordinate direction. Taking $\bar{X}$ as the computational coordinate, $0 \leq \bar{X} < 1$, the stretched coordinate is defined as

$$X = \begin{cases} \bar{X}_m & \bar{X} \leq \bar{X}_m \\ \bar{X}_m + B * C^A * (1-\bar{X}_m)\bar{X}_p/(C-\bar{X}_p^2)^A & \bar{X} > \bar{X}_m \end{cases}$$

where $\bar{X}_p = (\bar{X} - \bar{X}_m)/(1 - \bar{X}_m)$, $\bar{X}_m$ being the point in computational space where the stretching begins; and A, B, and C are the stretching parameters. Infinite physical domains are obtained by setting C = 1, as in the original code, while C > 1 gives a finite domain. A set of stretching parameters is defined for each coordinate direction. These can be chosen along with appropriate values of $\bar{X}_m$ to construct a desirable mesh. Examples of two-dimensional sections of the mesh are given in figure 4, for infinite and finite domains.

Outer Boundary Condition. - To apply the condition defined by equation (10) and thereby set the values of the reduced potential on the outer boundary mesh points, a scheme is required for obtaining the induced velocity $\vec{V}_2$ at boundary points and for integrating these on the surface, B. The $\vec{V}_2$ velocity field is provided by the vortex lattice wake model which can be used to compute the induced velocity at any point, once the wake element strengths have been defined. A suitable path of integration was chosen: following the boundary of each finite difference x-y mesh plane, and along a reference line connecting the leading mesh points of the planes, as shown in figure 5. The convenient locations for evaluating the induced $\vec{V}_2$ velocities are at points midway between mesh boundary points, giving a trapezoidal type scheme for the integration.

In the computer program, the integration around the boundary of each mesh plane is done separately, followed by the spanwise integration to set reference values of the potential at each plane. Then the boundary values of all the planes are reconciled to this reference line. One value of the potential must be set arbitrarily, and it was chosen to be zero at the most inboard reference point.

To make the boundary value computation more efficient, the induced velocity calculation is performed only on those mesh cells corresponding to the coarse mesh, followed by the integration. The potential values are then interpolated onto the current mesh boundary (medium or fine mesh). This is not crucial to the operation of the program, but is done only as a way of speeding up this part of the calculation. A Lagrange three point interpolation scheme is used to give a smooth distribution of potential on the boundary surface. Though accuracy is lost in the integration on the coarse mesh, the method seems to work well as long as the interpolated values are smooth.

Blade Surface Condition. - Equation (11) is applied in exactly the same manner as in reference 28, but with the inclusion of the embedded velocity associated with the definition of equation (5). The method of enforcing the blade surface condition uses an image point system very common to finite difference solutions.

Kutta Condition, Wake Fitting, and Roll-up. - The convection relation equation (12) is employed by defining a local jump in potential across the wake surface. The wake surface of the finite difference mesh is originally the branch cut originating at the trailing edge. This branch cut exists because the potential flow cannot contain any vorticity; hence, the solution region must be singly connected and envelop the blade and wake. The branch cut is termed here the "cut-surface." The cut-surface then has upper and lower surfaces across which there is a discontinuity in potential for lifting flows.

Since the cut-surface in the finite difference solution represents the wake surface, it is appropriate to make it consistent with the lattice wake, in terms of geometry and strength. To do this, both the vertical position and distribution of circulation on the cut-surface are made consistent with the lattice wake geometry by means of a linear interpolation. The resulting cut-surface shape is then more realistic than the usual flat wake of most finite difference codes. An example is shown in figure 6. It should be noted that this wake fitting procedure approximates the wake roll-up since the prescribed wake geometries have both a circulation strength and position which can result in a contraction and redistribution of the wake strength in a prescribed manner.

Coarse, Medium, Fine Mesh Levels. - To speed convergence the potential equation is solved in a sequence, first on a coarse mesh (e.g., 20 chord x 4 normal x 8 span cells) then on a medium mesh which has twice the cells of the coarse mesh (40 x 8 x 16) and lastly on a fine mesh which has again twice the cells of the previous mesh (80 x 16 x 32). This process is also referred to as grid halving or mesh refinement. To go from one mesh to the finer one, it is necessary to interpolate the solution onto the finer mesh so that the finer solution can begin with a nearly converged potential field. This is a common technique in finite difference methods. In the vortex lattice wake structure used here, the number of spanwise lattices is the same as the number of spanwise finite difference cells on the blade. This is convenient from a programming standpoint, but is probably unnecessary for adequate resolution of the wake influence.

Wake Model

Vortex Lattice. - A simple lattice type wake model is used, where the lattice is constructed by assembling individual elements. Each element is a four-sided vortex box, with the sides of the box being straight, constant strength Biot-Savart vortex segments. This choice of wake element assures that the resultant velocity field of the entire wake will be irrotational, since the box elements meet this requirement individually. Thus, the wake is consistent with the inner/outer domain formulation given above, both for the embedded portion and for the wake outside the inner domain. By treating the wake elements this way, the distinction between embedded elements and those outside is more easily made, and the program logic is simplified. In

addition, the circulation strength of each box is equal to the blade bound segment strength at the instant in time (azimuth position) it was created. Note that in the calculation of the wake influence it would be computationally efficient to consider the wake as made up of individual segments rather than boxes, but that the ease of coding and debugging was considered more important in the current effort.

Geometry. - The vortex lattice starts at the blade quarter chord location. There is one line of boxes along the blade, representing the lifting-line of the blade. The wake then starts at the trailing edge, and continues as far as specified. Any number of blades may be used, each being represented by an appropriate array of vortex boxes.

The geometry of the wake can, in principle, be prescribed by any method. It is convenient, however, to limit the selection of wake geometry models to a few of those that are currently in use and that can be generated easily. The models used in this investigation are

1. Hover -- The generalization of Landgrebe (ref. 6) extended to include the refinements of Kocurek and Tangler (ref. 9).

2. Forward Flight
   a. Classical Skewed Helix
   b. Generalization of Egolf and Landgrebe (ref. 14)

An example of a hover wake lattice is shown in figure 7. The inboard sheet is shaded. Note that the connecting lattices between the sheet and the tip have no net strength because there is no azimuthal variation in circulation strength. A forward flight wake is shown in figure 8 for an advance ratio of 0.1. For clarity, only the tip lattices are shown; the inboard sheet is a classical skewed helical surface. The convection velocity of the forward flight wake model used here is taken to be the momentum value, defined for example in reference 31. The generalized wake is an approximation to a distorted wake.

Ring Vortex Far Wake in Hover. - A ring vortex far wake model is provided in the analysis for hover applications. Typically only a few revolutions of the full vortex lattice are needed to resolve the details of the near wake effects, and the remaining wake influence can be represented by a series of circular ring vortices modeling the tip vortices. In the current analysis, these vortices are spaced axially according to the rate of axial displacement of the prescribed tip vortices.

Azimuthal Variation of Wake Strength in Forward Flight. - In forward flight the wake strength varies azimuthally as the blade circulation changes. This phenomenon is important in computing the correct wake induced flow at the

blade surface. Presently, however, the computer program does not sweep in azimuth to generate the wake; rather, the quasi-steady flow is solved for at a particular azimuth position. The current analysis is capable of using any distribution of blade bound circulations; these can be prescribed from any source. The present results were produced using a prescribed distribution of wake strength computed by a separate program, F398SR of reference 32. An example of the circulation distribution for a representative case (2-bladed rotor, 0.3 advance ratio) is shown in figure 9. For rotors with multiple blades, all blades except the one on which the finite difference solution is obtained have their bound circulations set by interpolation from the input array of wake strengths. At each update of the wake influence, the basic distribution defined by F389SR is re-scaled so that the peak circulation at the reference blade azimuth equals that of the ROT22/WAKE solution.

Roll-up of the Generalized Wake Tip Vortex. - A roll-up model is included in the generalized wake option. This model is quite simple, merely coalescing the lattices outboard of the point of maximum circulation. This roll-up is currently set to occur over the first 30-deg of wake age.

SOLUTION PROCEDURE

The basic flow diagram of the solution procedure is provided in figure 10. The required input information includes the airfoil ordinates, rotor planform, flight condition, the finite difference mesh parameters and relaxation coefficients. The analysis uses three levels of grid halving (coarse, medium, and fine) as mentioned before.

Iteration Process

Briefly, the process consists of an outer iteration loop corresponding to a grid halving loop and an inner loop in which the finite difference solution and wake geometry/influence are iterated to convergence on the current mesh. Within the solution loop, the finite difference portion of the analysis can be run for any number of relaxation sweeps between updates of the wake geometry and strength (refs. 28 and 29 provide details of the finite difference relaxation scheme.) To start the process, the initial mesh and wake geometries are computed from input quantities. An initial estimate for the finite difference blade boundary condition is made. This is normally the coarse grid. The solution process is entered, and the finite difference relaxation is applied for a number of sweeps (e.g, 10) to establish an approximate blade loading. Then an estimate of the rotor thrust (needed as input for the wake geometry calculation) is made based on the blade loading. New wake and mesh geometries are computed, and the wake strengths are determined from the trailing edge circulations of the finite difference solution. The embedded wake influence, $\vec{V}_1$, is computed and stored at each of the interior finite difference mesh points. This includes the derivatives of the velocity needed in equation (6). The vortex lattice method is then used to compute the external wake influence, $\vec{V}_2$, at the outer boundary of the finite difference mesh to provide the boundary values by equation (10). The solution is checked for convergence (currently, this check is made on the maximum correction to the finite difference solution). If the solution is converged to within the prescribed tolerance for this grid level, or if the limit of relaxation sweeps has been reached, the mesh is refined and the process repeats.

The frequency with which the wake influence is updated can be prescribed. On the fine meshes, it is desirable from a computation cost standpoint to limit the number of wake updates. This is because the number of embedded wake elements is currently related to the number of spanwise mesh points (all other parameters held fixed). The coarse and medium mesh wake updates are inexpensive and are permitted every time the peak circulation grows by 5%. By the end of the medium mesh solution, the blade load is fairly close to the final result; thus, the wake position is well established by the time the final mesh is entered.

Computation Time

The cost of evaluating the embedded wake influence can be a substantial part of the total computation time for a method of this sort. This is because the embedding procedure requires that the wake element velocities and their derivatives be computed at each of the finite difference mesh points. (It would be possible, and perhaps efficient, to compute the $\vec{V}_1$ influence only at points on solid boundaries and where the local Mach number is high; but this would require logical tests that could prove cumbersome.) In fact, for some cases there may be enough wake elements inside the inner domain that the embedding costs dominate the calculation. Clearly, the smaller the inner domain, the better; but transonic conditions at the tip put a limit on the proximity of the outer boundary.

For the present analysis, the computation time is presented as two parameters: the cost to evaluate the embedded velocities and derivatives, and the basic cost of the finite difference relaxation algorithm. The current calculations were performed on a Perkin-Elmer 3200 series super-minicomputer (approximately the same speed as a Digital Equipment Corporation VAX 780). The CPU time required to compute the influence (velocity and velocity gradient) of one four-sided vortex box wake element at one mesh point is about 0.0035 sec. The time required for one relaxation sweep is about 0.0017 sec per mesh point. From these values an approximate relation can be given for the proportion of time devoted to the embedding procedure relative to the finite difference solution portion:

$$P = 2 * \frac{[\text{Number of Embedded Wake Elements}]}{[\text{Number of Finite Difference Sweeps per Wake update}]}$$

This estimate is probably valid for similar methods using the vortex box wake element, and a full potential relaxation scheme on a scalar processing computer. Assuming that the frequency of the updates is known and fixed, then the number of embedded wake elements is the important parameter. This can be controlled in two ways: either by making the inner domain small so as to exclude as many elements as possible, or to change the coarseness of the wake lattice.

VERIFICATION OF CONCEPT

The complexity of helicopter rotor aerodynamics makes the verification of a particular method very difficult. Here, three demonstrations are presented as verification of the two basic aspects of the current method: 1) the inclusion of the external ($\vec{V}_2$) wake influence by the boundary integration, 2) the inclusion of the remaining wake influence by the technique of vortex embedding, and 3) the result of these techniques in producing the wake influence on rotor airloads. The first demonstration compares an infinite domain (unaltered ROT22) case with two finite domain cases. One of the finite domain cases uses the boundary integration and one has the reduced potential set to zero on the outer boundary. The original ROT22 code recognizes only one quarter of a wake revolution shed off the blade. As such, all three cases used 1/4 revolution of wake, so that there was no embedded portion and so that the cases correspond to the usual ROT22 treatment. Figure 11 shows the radial load distribution on a blade in hover for these cases. The finite domain case with the boundary values determined by the integration described above is essentially the same as the infinite domain case. The small differences noted are due to the lack of a thickness model, numerical integration errors, and the associated discrete vortex lattice wake model. The finite domain case with zero prescribed as the outer boundary condition is clearly incorrect. This is directly analogous to the lack of a far field lift model in finite domain two-dimensional calculations. Thus, the influence of the blade and its associated wake can be included through the boundary conditions (for those portions of the wake which are entirely 'external' to the finite difference domain).

The vortex embedding concept is demonstrated in figure 12, where residual flow vectors are shown indicating the influence of the embedded portion of the wake. This residual field is that of a complete rotor and wake solution with embedded vortex wake elements, minus that of the rotor with only the basic ROT22 1/4 rev of wake. In figure 12 the approximate path of the wake of the preceding blade (2-bladed rotor), is shaded. Near this path, the flow disturbance due to the discrete model of a wake sheet is evident. These results indicate that the fundamental aspects of the concept function correctly.

Further evidence is provided in a more specific example which exhibits the general blade loading features due to the influence of the wake of a lifting rotor. In figure 13, the effect of both the local influence of a tip vortex and the global wake influence are demonstrated. The local tip vortex influence results in the characteristic spanwise circulation distribution for hover (fig. 13a). The global influence of the wake due to two blades results in a general downwash which reduces the blade loading (fig. 13b).

Thickness Effects on the Outer Boundary Condition. - As noted earlier, thickness effects are neglected for the determination of the boundary conditions on the outer surface of the inner domain. Because the thickness disturbance in transonic flows is dramatically greater than in subsonic flows, the question arises as to the need for a thickness-type correction to the boundary condition for accurate transonic calculations using the finite domain. Investigations were made using two-dimensional transonic small disturbance theory and also the three-dimensional full potential analysis of reference 29 for a limited number of Mach number conditions which were representative of rotor tip Mach numbers. It was found that the inclusion of a thickness model was necessary in most transonic two-dimensional calculations on meshes whose outer boundaries were within a few chord lengths of the airfoil. However, for the three-dimensional wing analysis, the Mach number could be larger than in the corresponding two-dimensional case because of three-dimensional relief.

This investigation was continued into the three-dimensional rotor problem. A non-lifting test case at high tip speed ($M_{Tip} = 0.65$) and high advance ratio (0.4) was run using both the infinite and finite domain meshes shown in figure 4. This represents a severe operating condition with maximum tip Mach number 0.91. The resulting blade surface pressure distributions are given in figure 14. Since the case is non-lifting, the wake has no effect on the boundary condition (which is zero for both domains). Thus, the discrepancy between the two cases is due to the thickness alone. This discrepancy is evident on the outboard stations for this extreme operating condition. As a result it is felt that for conditions of this severity combined with a finite domain such as used here, a thickness model should be used. For more usual Mach numbers, or for larger domains, the thickness effect will be secondary to the lift effects accounted for by the wake method given here. Based on these results it is felt that the current model for the calculation of the boundary conditions is adequate for all but the most severe conditions.

APPLICATIONS

The preceding section illustrated verification of the fundamental aspects of the technical approach and the general features of the wake influence. In this section the results of several applications to both hover and forward flight are presented. Correlations with data in hover for both subsonic and transonic lifting conditions are presented. These results demonstrate that the method is properly accounting for nonlinear transonic flow effects (inviscid) and the wake influence.

A forward flight correlation study consisting of a comparison of theoretical results with test data was beyond the scope of this contract activity. Earlier correlations with data, both blade surface and field information, have been shown with the ROT22 analysis for non-lifting transonic forward flight conditions (refs. 28 and 33). A theory-test comparison has recently been completed as part of the ongoing UTRC research program, and the results of this comparison are presented in reference 34 for an Army 1/7-scale model rotor at two advanced ratios, 0.298 and 0.345. These results demonstrate that the code is capable of modeling the transonic aspects of forward flight conditions. The forward flight applications shown herein are presented to demonstrate the influence of the wake modeling in forward flight.

All of the results presented, unless otherwise noted, used a finite difference mesh of 80 x 16 x 32 cells, and two revolutions of vortex lattice wake.

Hover

With the inner/outer domain formulation verified, the analysis was applied to several hover test configurations for which data are available. Conditions from two different sources of data were obtained to provide a reasonable range of correlation. (These hover results have also been presented in reference 35. In that reference the cases were originally run with a single finite length vortex to model the tip vortex influence. Also the portion of the inboard sheets which passed into the finite domain was neglected. Since that time the single finite length vortex and missing portions of the sheets have been replaced with the complete hover generalized wake structure. The results of the more accurate wake structure showed only a slight change in the loading, pressure distributions, and required only a small change in blade collective setting to match the thrust condition. As such, the results shown herein are reproduced directly from ref. 35.) In the hover applications shown, ten revolutions of ring vortex far wake were used.

Single Bladed Rotor, Low Tip Speed. - To validate the capabilities of the analysis as applied to an actual rotor condition for which quality chordwise pressure distributions were available, the analysis was applied to the model

rotor test conditions of reference 36. In that test program, a low aspect ratio (4.8), single-bladed rotor was run at one tip speed (0.25 Mach number) and three collective pitch angles (0, 6.18, and 11.4 degrees) using two different square tip end shapes (flat and half body of revolution). The blade was untwisted and of constant chord, having a NACA-0012 airfoil section. Data are available at the 0.94, 0.966, 0.980, 0.987, 0.991, and 0.995 R stations, providing detailed chordwise pressure measurements in the tip region. In this application, the ROT22/WAKE analysis was run using the test values of collective pitch. Comparisons with the ROT22/WAKE results are given below. Since the mesh structure of ROT22 is incapable of resolving the actual tip end shape (not to be confused with tip planform shape), the data for the half body of revolution tip are used for comparison. There is little difference in the experimental data for the two end shapes, except very near the tip.

The predicted and experimental pressure distributions (C_p) are shown in figure 15 for all blade angles reported in reference 36. The measured data shown on these plots are for the 0.940, 0.966, and 0.987 radial stations. The computed results are for the 0.944, 0.967, and 0.989 radial stations. Excellent agreement between the measured and predicted distributions at the 0.94 and 0.966 radial stations was obtained for all blade angles. The agreement at the 0.987 radial station is surprisingly good for a potential method. These results indicate that the analysis accurately predicts the fundamental features of the rotary wing flow problem.

Although the agreement for this application is very good, the model rotor considered is single bladed and thus the wake and the passing tip vortex influence are generally weaker than for conventional rotors. Also, the limited spanwise data prohibits comparison at inboard stations and the conditions were subsonic. The second application provides an additional measure of the predictive capabilities of the analysis.

Two Bladed Rotor, High Tip Speed. - The second source of data used for comparison is that of reference 37, being the results of a model rotor test in hover for a range of tip speeds. This test provided chordwise pressure measurements and spanwise load information at five stations from midspan to the tip. The tip Mach number conditions ranged from 0.266 to 0.877. The rotor used in the test was a two-bladed, untwisted, constant chord model with aspect ratio 6.5. The blade section was a NACA-0012. Measurements were made at various collective pitch settings from 0 to 12 degrees. ROT22/WAKE results are compared with several of the test conditions. For each of these conditions, the analysis was run to give approximately the same thrust as reported from the test. The ROT22/WAKE pitch settings were 1-2 degrees lower than the test values for this two bladed rotor. For the previous case (rotor of ref. 36), however, good correlation was obtained using the measured pitch angles.

The first case is a low tip Mach number condition (0.439). The second is a high tip Mach number case (0.877). Third, the effect of Mach number is considered at a particular station near the tip, at a fixed collective pitch. Finally, a comparison is made for a high collective pitch setting (12-deg) at a high tip Mach number (0.794).

The low tip Mach number case (0.439) is presented in figures 16 and 17. Figure 16 shows the measured and predicted spanwise distributions of section lift coefficient. The load distribution as predicted by ROT22 is shown here, both with and without the wake influence. Where no wake is included, the prediction is obviously deficient. The inclusion of the wake model results in generally good agreement between the measured and computed load distributions. For comparative purposes a calculation from reference 37 is included in figure 16. This result is based on the lifting-surface method of reference 13 using the measured tip vortex geometry from the test. In reference 36 additional lifting-surface predictions were made with adjusted wake geometries which in some cases improved the correlation.

A comparison of the computed with the measured chordwise pressure distributions at the five radial stations is shown in figure 17. The correlation is good, particularly at the outboard stations.

The higher Mach number condition resulted in very similar correlation, as shown in figure 18. This condition shows the ability of the analysis to predict the transonic flow on the blade. For additional comparison, the measured results presented in reference 37 at the 0.8R station are reproduced in part in figure 19 along with the current ROT22/WAKE prediction and those computed results from reference 37 based on a two-dimensional finite difference method. The lifting-surface analysis noted earlier was used to provide an estimate of the section angle-of-attack for the two-dimensional calculation. Both an inviscid and a viscous two-dimensional computation are compared with the test result. The inviscid conservative method gives a shock that is too strong, while the equivalent viscous calculation shows excellent agreement with the data. While ROT22/WAKE has no viscous correction, it is formulated in the non-conservative fashion which tends to smear the shock.

The effect of tip Mach number on the character of the chordwise loading distribution is shown in figure 20. Four tip Mach number conditions (0.439, 0.612, 0.794, and 0.877) were computed for the 8.0 degree collective pitch condition. The pressure distributions are shown for the 0.96 radial station. The capture of the shock is evident for the increased Mach number. This feature is well predicted by the analysis.

One further condition was run to compare with test results. The test condition was a high blade collective pitch setting of 12.0 degrees, run at a tip Mach number of 0.794. The comparison of the measured and predicted pressure distributions is shown in figure 21 for this case. No evidence of stall is noted. Again, the correlation is quite good, although some differences are seen in the peak pressure coefficients on the three innermost radial stations.

Forward Flight

As noted above, a forward flight correlation with experiment is beyond the scope of the current effort. Here we present some computed results for two flight conditions of a two-bladed rotor for demonstration purposes. The simulation used a constant section, constant chord, untapered, unswept blade with a linear twist of -10 degrees. The rotor radius to chord ratio was 9.22. A NACA Four-digit symmetrical airfoil was used with 9.7% maximum thickness. The two conditions are for advance ratios of 0.2 and 0.35.

To indicate the effect of the presence of the wake, cases were run using the generalized wake (ref. 14), the classical skewed helical wake, and the original infinite domain ROT22 analysis. The results for the 90 deg blade azimuth position are shown in figure 22. The infinite domain version of ROT22 which used only one-quarter revolution of wake, for one blade, predicts higher inboard loading and demonstrates no effect of the wake of the preceding blade on the loading. The generalized wake case reveals the dramatic influence of the concentrated passing vortex near the tip when compared with the classical wake model. This comparison clearly indicates the need for the inclusion of the wake model.

Moderate Advance Ratio, $\mu = 0.2$. - Further studies of the effect of the wake model are shown in figure 23 for the moderate advance ratio condition. Load distributions are given in figure 23 for the rotor blade at three azimuth positions, 60, 90, and 120 deg. The angle-of-attack of the tip-path plane was set to -4 deg, and the rotational tip Mach number was 0.66. Results are shown for both the generalized wake and classical skewed helical wake to indicate the strong influence of the wake geometry model on the solution. The location of a strong tip vortex influence is seen to move in the inward radial direction as the blade advances in azimuth position. The generalized wake is usually closer to the blade in this azimuth range than the corresponding helical wake, and the generalized wake model used here has a rolled up tip vortex, making the influence quite strong near the tip vortex passage. It is noted that the characteristic features of the airload distributions in figures 22 and 23 regarding the existence and locations of local peaks are consistent with those observed in measured H-34 rotor airloads of reference 38.

Blade surface pressure distributions are presented in figure 24 for the 90-deg azimuth case. Four radial stations are shown: 0.60, 0.75, 0.88, and 0.96. As seen from the figure 23, the primary tip vortex interaction occurs at about 0.9R for this condition (generalized wake); the pressure distribution nearby (0.88R) is strongly affected relative to the classical wake result. The close vortex passage has resulted in a significant aft loading creating a large nose-up section pitching moment. Lack of closure of the pressure distributions at the blade trailing edges for close vortex passages (tip and inboard sheet) is exhibited in this figure (r/R = 0.756). This has been identified as being related to the manner in which the original analysis incorporates the boundary condition across the cut-surface. This anomaly has not been seen in the hover applications where the inboard sheet is further removed from the blade and the tip vortex is further outboard. Given the inviscid nature of the method, correcting this aspect of the model for close blade/vortex interactions was beyond the scope of this research program.

High Advance Ratio, $\mu = 0.35$. - This case represents a transonic tip speed condition. Blade loadings are shown in figure 25. Again note the very marked difference in the generalized wake result compared to the classical wake at the 90 deg azimuth location. Here the primary vortex passage occurs approximately 25% closer in the case of the generalized wake than for the classical wake. The tip vortex is rolled up for the generalized wake model. The vortex passage occurs at about 0.6R, as born out by the load distribution.

The corresponding pressure distributions are given in figure 26. These are for the 90 deg azimuth case. The difference between the two wake models is most evident at the 0.6R station, especially on the lower side. Outboard the flow is transonic and shock waves are present.

To see the change in surface Mach number distributions over the azimuth sweep, 60, 90, and 120 deg, the Mach contours are given in figure 27 for the 0.35 advance ratio case. The outer 25% of the blade is shown, with both upper and lower surfaces. Of the three azimuth positions, the region of supersonic flow is seen to be a maximum at the 90 deg azimuth position.

DISCUSSION OF RESULTS

From the results presented for both hover and forward flight application, it is evident that the approach defined herein provides for the treatment of helicopter rotor wake modeling in a finite difference code in a cost effective and accurate manner within the assumptions of inviscid theory and the accuracy of the wake models. The method has been shown to provide for the nonlinear transonic flow effects along with the local and global wake influence. The results are sensitive to the accuracy of the wake models. Wake modeling techniques are currently more advanced for hover than for forward flight. As a result, validation in forward flight is still required. There are of course other areas which require additional study and or refinements. Some of these are addressed below.

Efficiency. - As mentioned above, the run time can be dominated by the embedded wake influence calculations. One way to reduce this time is to provide a faster calculation of the influence of individual wake elements. The point doublet representation of the wake element is adequate for far-field influence and is about 2.5 times faster per evaluation than the vortex-box module. This model could be easily incorporated in the analysis. A different way of computing the box influence would be more efficient, as well, but the ease of coding in the present method seemed to be a greater benefit in the research study.

Another way to improve the efficiency of the embedded wake calculation is simply to reduce the number of wake elements. Currently, the number of spanwise wake elements is equal to the number of spanwise finite difference cells on the blade. This is probably not necessary; the number of wake elements needed to resolve the flow field may be less than used here on the fine mesh solutions (22 along the blade), and certainly they could be distributed in a way that would make the most efficient use of them.

Yet a third way to speed the embedding part of the method is to make the inner domain as small as possible. Along with reducing the number of embedded elements, this also reduces the number of grid points. However, reducing the physical size of the inner domain can lead to problems in transonic flow and may require a distributed blade loading model in place of the lifting-line model for the calculation of the boundary conditions on the outer surface of the inner domain.

Transonic Thickness Effect. - The thickness disturbance in transonic flows is dramatically greater than in subsonic flows. Although the earlier studies indicated that the lack of a thickness model was acceptable for the size of the current domain, reduction in the domain size would be desirable.

Studies to incorporate thickness effects in the calculation of the boundary conditions are required. Such a model would also have to be based on compressible flow theory.

Distributed Lift Model. - A lifting-surface or panel method could be incorporated to replace the lifting-line model for the blade lift when calculating the boundary conditions on the outer domain. This feature is not currently needed, but if the inner domain size is reduced, it may be. Such a model would result in increased cost for the calculation of the boundary conditions, but the cost for the finite difference portion of the code would be reduced. Trade-off studies would be required.

Compressible Wake Model. - The current lifting-line/wake model is based on incompressible flow. The results presented for transonic hover conditions indicate that the incompressible lifting-line/wake model is a good approximation for the wake effects. This is believed to be attributable to two reasons. First, though the spacial variation of induced velocity is different for a vortex in linear compressible flow than for one in incompressible flow, the net circulation is the same (the strengths being equal). Second, the velocity potential of a vortex in three-dimensional flow attenuates more rapidly with distance than in two dimensions. Thus, where a two-dimensional finite domain calculation would require the compressible vortex model, the three-dimensional flow at the same Mach number might not, depending on the domain size. Thus, inclusion of compressibility in the wake and lifting-line (lifting-surface or panel) models should be considered if the domain size is reduced.

Convergence. - How often the wake influence should be updated is not fully known. Thus far it seems that adequate convergence is obtained by re-evaluating the wake influence every time the peak circulation grows by 5%, except on the fine mesh (which is the final stage of the computation) where only one update is allowed.

Lattice Structure/Roll-up. - It has become evident to the investigators that treating the wake as a single array of interconnected elements is convenient computationally but does not lend itself easily to the problem of roll-up. A more suitable way of handling the wake might be to use two independent arrays for the geometry, one for the inboard sheet and one for the rolled up tip lattices. The wake strength would be handled in the same way.

Vortex Core Model. - The embedded vortices currently use a core radius equal to ten percent of the blade chord. It was convenient to develop the embedding procedure first for irrotational embedded fields, though the use of a core model violates this for any points within the core. The extension to rotational embedded fields is straightforward but would require thorough analysis.

Cut/Wake-Surface Boundary Conditions. - As noted earlier, there are some discrepancies on the pressure distributions on the blade trailing edge for conditions where the wake passes close to the blade. This is attributable to the implementation of the boundary condition across the cut-surface over several grid points. This area should be addressed in future research work.

Improved Wake Sheet Model. - The current wake model uses vortex singularities to model the inboard wake sheet. For near wake sheet/blade interactions the use of discrete vortex filaments is not appropriate. During the course of this investigation, some conditions where the inboard sheet passed very close to the blade resulted in erroneous loading predictions. One simple solution is to use more filaments and/or include vortex cores for the sheet filaments. However, the complexities of the coding and the cost for the embedded calculations makes this approach unattractive. An alternate approach would be to use vortex panels in place of the vortex filaments. Although the cost per panel is higher than the cost per vortex element (box), the panels could be larger and reduce the number of embedded calculations. Studies in this area are warranted.

Quasi-steady Assumption. - Although there is some concern related to the validity of using quasi-steady methods for forward flight, it has been demonstrated to yield reasonable predictions for non-lifting conditions, references 28 and 33. It remains to be seen over what range of conditions (advance ratio, loading) the quasi-steady steady assumption is useful for general predictions.

CONCLUDING REMARKS

A method of including rotor wake effects in a full potential method has been developed and demonstrated for both hover and forward flight applications. The full potential flow method (ROT22/WAKE) is based on the solution of the quasi-linear form of the potential equation and applied in a quasi-steady manner to rotor flows. The inclusion of the wake influence using the inner/outer domain concept with prescribed wake geometries and the embedded vortex features is also adaptable to more advanced methods, such as Euler codes and unsteady flow solvers.

This method of solution has the advantage of reduced volume for the nonlinear inner domain solution (finite difference) while treating the global influence of the complex rotor wake with a linear solution method based on prescribed wake models. Finite inner domain solutions also have the advantage of minimizing the number of embedded vortex elements, a feature which can potentially provide large computer cost savings.

The use of the prescribed wake method allows for realistic wake geometries to be used in the solution process. The applications in hover have demonstrated successful correlation of blade airloads with test results for conditions for which realistic wake geometry models are readily available in both subsonic and transonic flow conditions. Although forward flight correlations have not been performed under this research activity, the analysis has been shown to predict the influence of various forward flight wake models for both subsonic and transonic lifting conditions.

The analysis as developed is currently a research tool. Further refinements can be made to improve the numerical efficiency of the method and enhance the rigor of some of the assumptions used in this initial study. However, it is evident that the approach is cost effective and can provide a tool for modeling realistic rotor wake influence in finite difference analyses for the prediction of rotor airloads.

REFERENCES

1. Gray, R. B., "On the Motion of the Helical Vortex Sheet Shed from a Single-Bladed Hovering Model Helicopter Rotor and its Application to the Calculation of the Spanwise Aerodynamic Loading," Princeton Aeronautical Engineering Dept. Report No. 313, September 1955.

2. Gray, R. B., "An Aerodynamic Analysis of a Single Bladed Rotor in Hovering and Low Speed Forward Flight as Determined from the Smoke Studies of the Vorticity Distribution in the Wake," Princeton Aeronautical Engineering Dept. Report No. 356, September 1956.

3. Landgrebe, A. J., "An Analytical Method for Predicting Rotor Wake Geometry," Journal of the American Helicopter Society, Vol. 14, No. 4, October 1969.

4. Landgrebe, A. J., "An Analytical and Experimental Investigation of Helicopter Rotor Hover Performance and Wake Geometry Characteristics," USAAMRDL TR-71-24, U. S. Army, June 1971.

5. Landgrebe, A. J. and Bellinger, E. D., "An Investigation of the Quantitative Applicability of Model Helicopter Rotor Wake Patterns Obtained from a Water Tunnel," USAAMRDL TR-71-69, December 1971. (AD 739 946)

6. Landgrebe, A. J., "The Wake Geometry of a Hovering Helicopter Rotor and Its Influence on Rotor Performance," Journal of the American Helicopter Society, Vol. 17, No. 4, October 1972.

7. Landgrebe, A. J. and Cheney, M. C., "Rotor Wakes - Key to Performance Prediction," Presented at the Symposium on Status of Testing and Modeling Techniques for V/STOL Aircraft, Mideast Region of the American Helicoter Society, October 1972; also "Aerodynamics of Rotary Wings," AGARD CP-111, February 1973, pp. 1-1 - 1-9.

8. Landgrebe, A. J. and Egolf, T. A., "Rotorcraft Wake Analysis for the Prediction of Induced Velocities," USAAMRDL TR-75-45, January 1976.

9. Kocurek, J. D. and Tangler, J. L., "A Prescribed Wake Lifting Surface Hover Performance Analysis," Proceedings of the American Helicopter Society 32th Annual Forum, May 1976.

10. Landgrebe, A. J. and Egolf, T. A., "Prediction of Helicopter Induced Flow Velocities Using The Rotorcraft Wake Analysis," Proceedings of the American Helicopter Society 32th Annual Forum, May 1976.

11. Landgrebe, A. J., Moffitt, R. C., and Clark, D. R., "Aerodynamic Technology for Advanced Rotorcraft," Journal of the American Helicopter Society, Vol. 22, Nos. 2 and 3, April and July 1977.

12. Moffitt, R. M. and Sheehy, T. W., "Prediction of Helicopter Rotor Performance in Vertical Climb and Sideward Flight," Proceedings of the American Helicopter Society 35th Annual Forum, May 1979.

13. Summa, J. M. and Clark, D. R., "A Lifting-Surface Method for Hover/Climb Airloads," Proceedings of the American Helicopter Society 35th Annual Forum, May 1979.

14. Egolf, T. A. and Landgrebe, A. J., "Helicopter Rotor Wake Geometry and Its Influence In Forward Flight - Volume I - Generalized Wake Geometry and Wake Effects on Rotor Airloads and Performance," NASA CR-3726, October 1983.

15. Egolf, T. A. and Landgrebe, A. J., "Helicopter Rotor Wake Geometry and Its Influence In Forward Flight - Volume II - Wake Geometry Charts," NASA CR-3727, October 1983.

16. Egolf, T. A. and Landgrebe, A. J., "Generalized Wake Geometry for a Helicopter Rotor in Forward Flight and Effect of Wake Deformation on Airloads," Proceedings of the American Helicopter Society 40th Annual Forum, May 1984.

17. Landgrebe, A. J., "Overview of Helicopter Wake and Airloads Technology," Proceedings of the American Helicopter Society/Nanjing Aeronautical Institute Seminar -- The Theoretical Basis of Helicopter Technology, November 1985.

18. McCroskey, W. J. and Goorjian, P. M., "Interactions of Airfoils with Gusts and Concentrated Vortices in Unsteady Transonic Flow," AIAA Paper 83-1691, July 1983.

19. Steinhoff, J., Ramachandran, K., and Suryanarayanan, K., "The Treatment of Convected Vortices in Compressible Potential Flow," AGARD-CP-342, 1983, pp. 22-1-22-12.

20. Tauber, M. E. and Hicks, R. M., "Computerized Three-Dimensional Aerodynamic Design of a Lifting Rotor Blade," Proceedings of the American Helicopter Society 36th Annual Forum, May 1980.

21. Tauber, M. E., "Computerized Aerodynamic Design of a Transonically 'Quiet' Blade," Proceedings of the American Helicopter Society 40th Annual Forum, May 1984, pp. 401-418. pp. 529-542.

22. Caradonna, F. X., Tung, C., and Desopper, A., "Finite Difference Modeling of Rotor Flows Including Wake Effects," Journal of the American Helicopter Society, April 1984.

23. Chang, I-C. and Tung, C., "Numerical solution of the Full-Potential Equation for Rotors and Oblique Wings Using a New Wake Model," Presented at the AIAA 23rd Aerospace Sciences Meeting, AIAA-85-0268, January 1985.

24. Sankar, N. L. and Prichard, D., "Solution of Transonic Flow Past Rotor Blades Using the Conservative Full-Potential Equation," AIAA Paper 85-5012, October 1985.

25. Strawn, R. C. and Caradonna, F. X., "Numerical Modeling of Rotor Flows with a Conservative Form of the Full-Potential Equations," AIAA Paper 86-0079, January 1986.

26. Roberts, T. W. and Murman, E. M., "Solution Method for a Hovering Helicopter Rotor Using the Euler Equations," AIAA Paper 85-0436, January 1985.

27. Sankar, N. L., Wake, B. E., and Lekoudis, S. G., "Solution of the Unsteady Euler Equations for Fixed and Rotor Wing Configurations," AIAA Paper 85-0120, January 1985.

28. Arieli, R. and Tauber, M. E., "Analysis of the Quasi-Steady Flow about an Isolated Lifting Helicopter Rotor Blade," JIAA TR-24, August 1979.

29. Jameson, A. and Caughey, D. A., "Numerical Calculation of the Transonic Flow Past a Swept Wing," ERDA Research and Development Report, Mathematics and Computing, June 1977.

30. Klunker, E. B., "Contribution to Methods for Calculating the Flow About Thin Lifting Wings at Transonic Speeds - Analytic Expressions for the Far-Field," NASA TN D-6530, November 1971.

31. Gessow, A. and Myers, G. C., Jr., Aerodynamics of the Helicopter, Frederick Ungar Publishing Co., New York, 1952, pp. 185-186.

32. Egolf, T. A. and Landgrebe, A. J., "A Prescribed Wake Rotor Inflow and Flow Field Prediction Analysis--User's Manual and Technical Approach," NASA CR-165894, June 1982.

33. Tauber, M. E., Chang, I-C., Caughey, D. A., and Philippe, J. J., "Comparison of Calculated and Measured Pressures on Straight- and Swept-Tip Model Rotor Blades," NASA TM-85872, December 1983.

34. Egolf, T. A. and Sparks, S. P., "Hovering Rotor Airload Prediction Using a Full Potential Flow Analysis with Realistic Wake Geometry," Proceedings of the American Helicopter Society 41st Annual Forum, May 1985, pp. 515-530.

35. Egolf, T. A. and Sparks, S. P., "A Full Potential Rotor Analysis with Wake Influence Using an Inner-Outer Domain Technique," Presented at the 42nd Annual Forum of the American Helicopter Society, June 2-4, 1986.

36. Gray, R. B., McMahon, H. M., Shenoy, K. R., and Hammer, M. L., "Surface Pressure Measurements at Two Tips of a Model Helicopter Rotor in Hover," NASA CR-3281, May 1980.

37. Caradonna, F. X. and Tung, C., "Experimental and Analytical Studies of a Model Helicopter Rotor in Hover," NASA TM-81232 (also USAAVRADCOM TR-81-A-23), September 1981.

38. Rabbot, J. P., Jr., Lizak, A. A. and Paglino, V. M., "A Presentation of Measured and Calculated Full-Scale Rotor Blade Aerodynamic and Structural Loads," USAAVLABS TR66-31, July 1966.

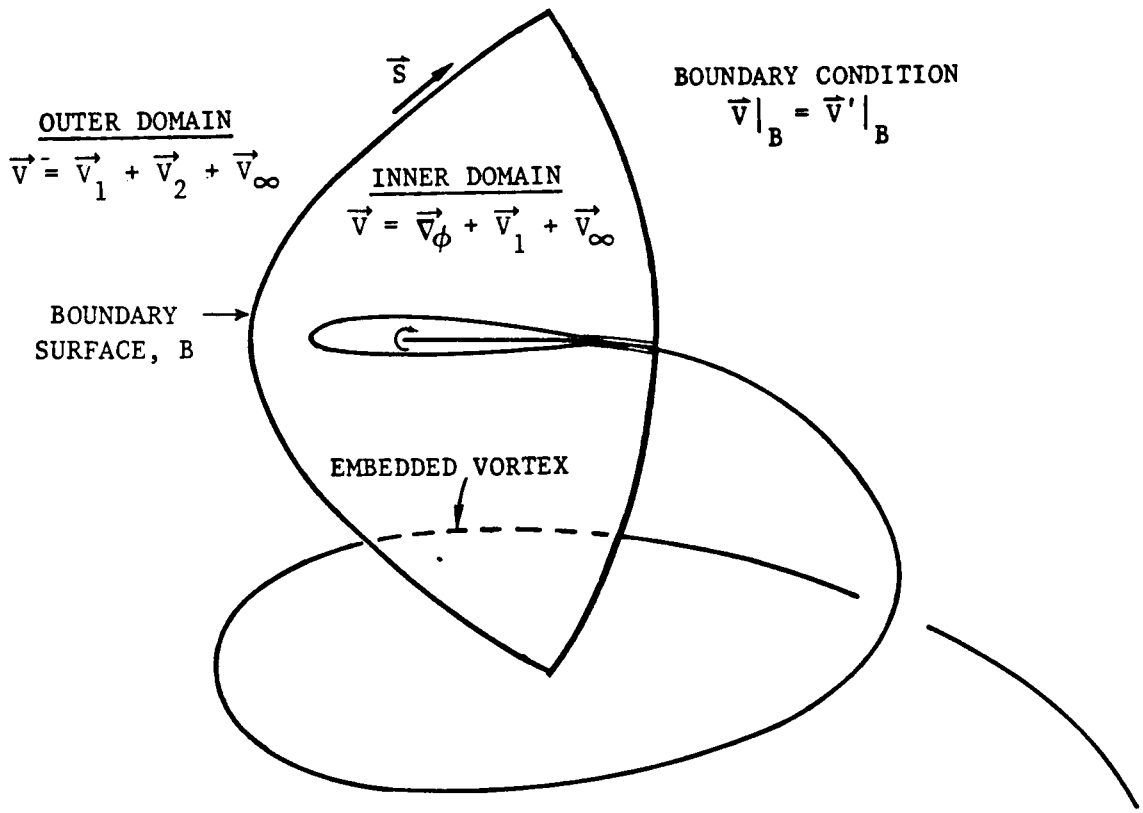

Figure 1 Schematic Illustrating the Inner / Outer Domain Formulation

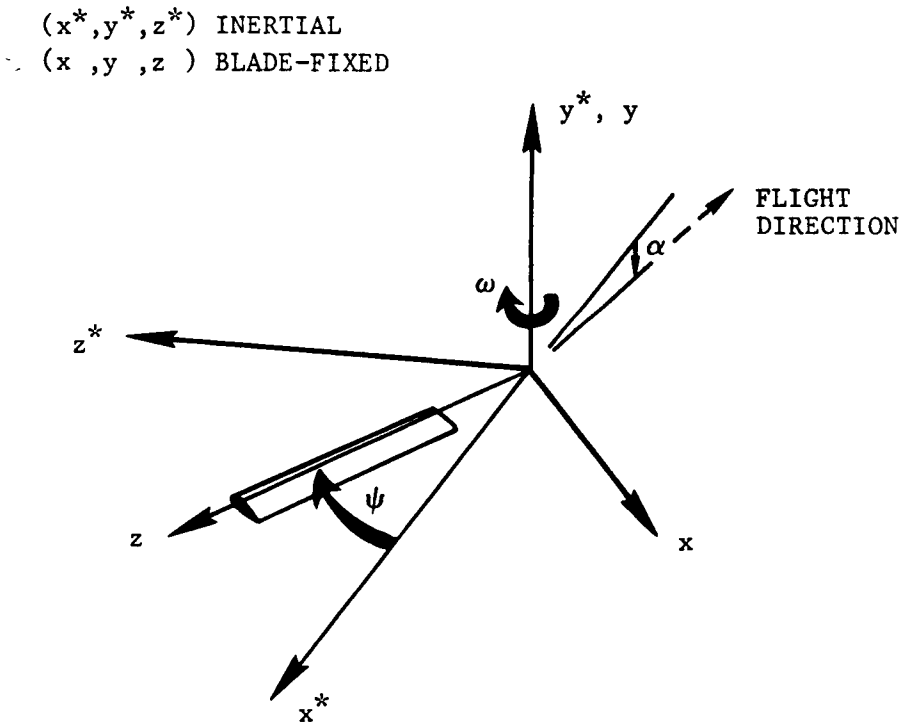

Figure 2 Rotor Coordinate System

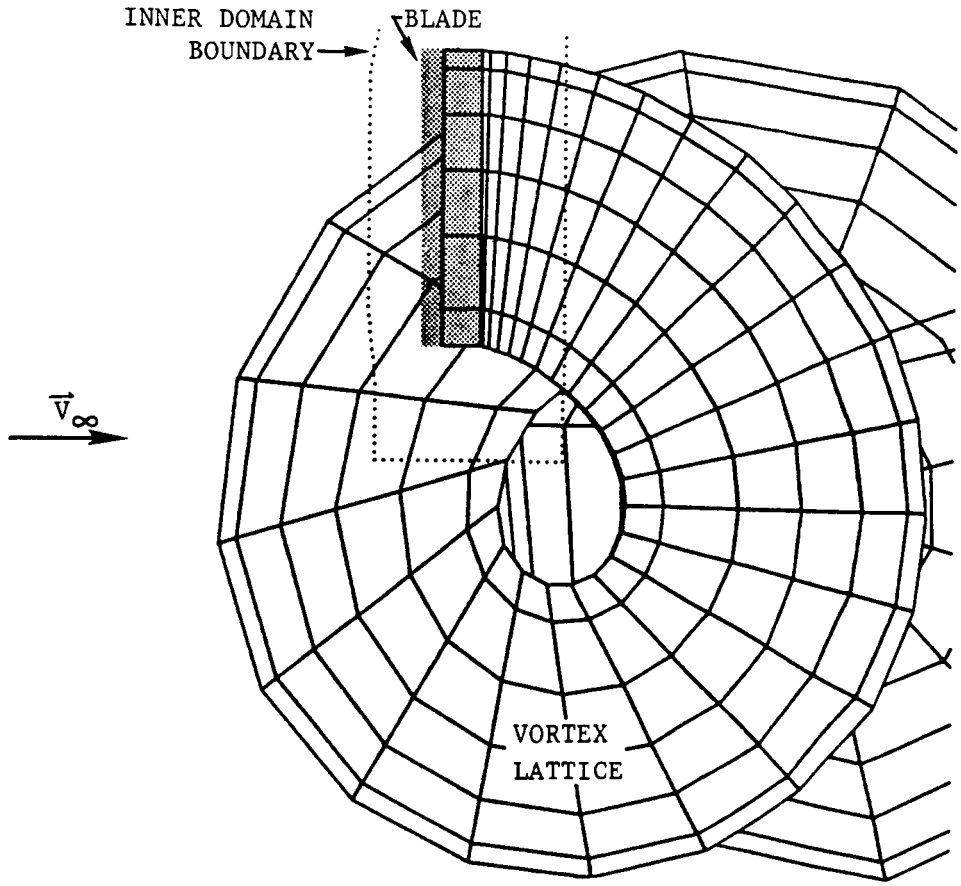

TOP VIEW

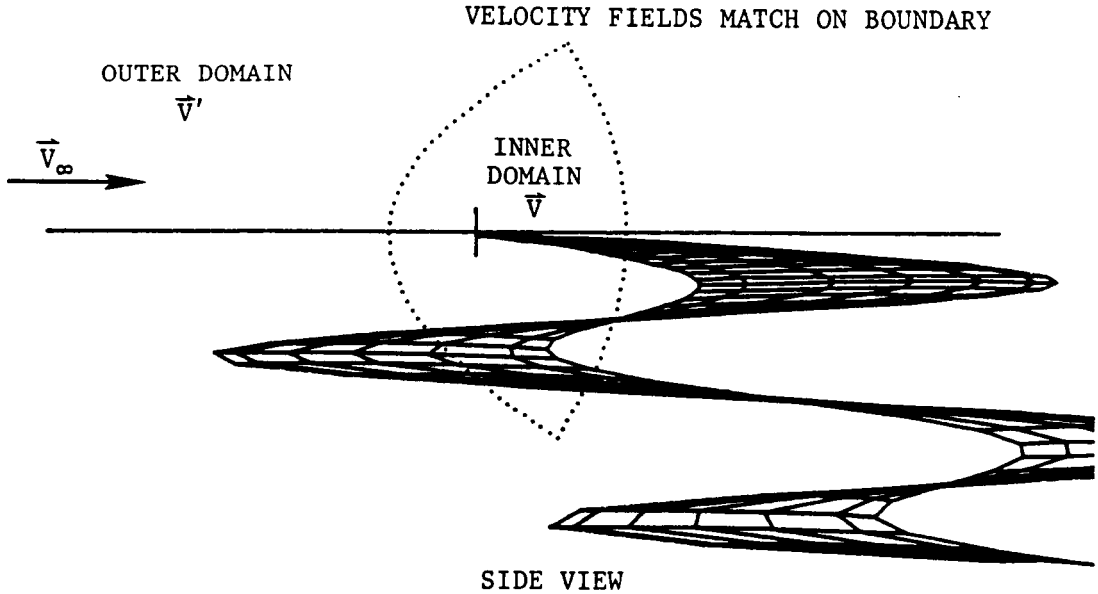

SIDE VIEW

Figure 3a) Inner / Outer Domain Showing Wake Lattice

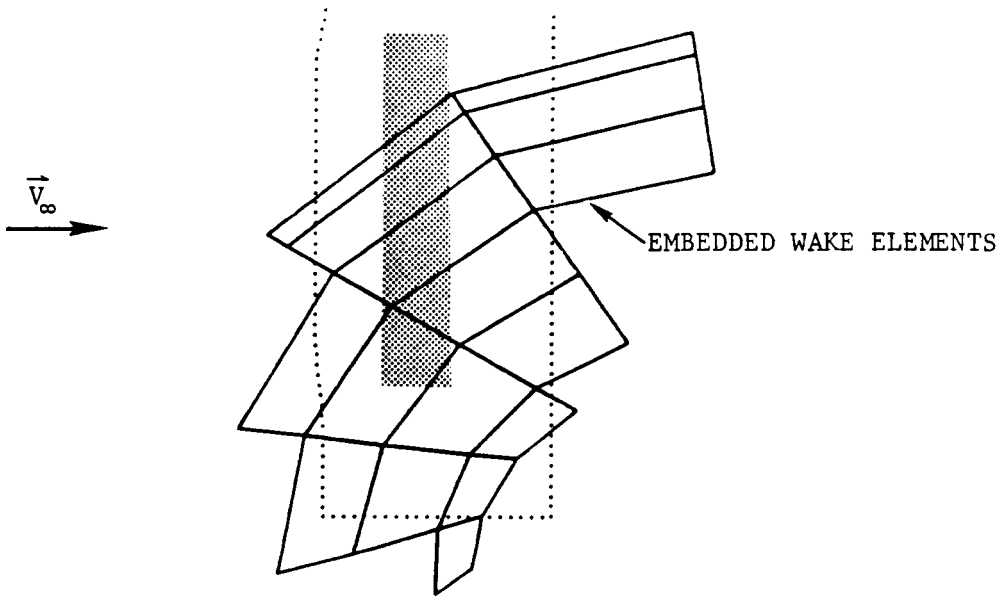

TOP VIEW

THE INNER DOMAIN SOLUTION IS
$\vec{V} = \vec{\nabla}\phi + \vec{V}_\infty + \vec{V}_1$

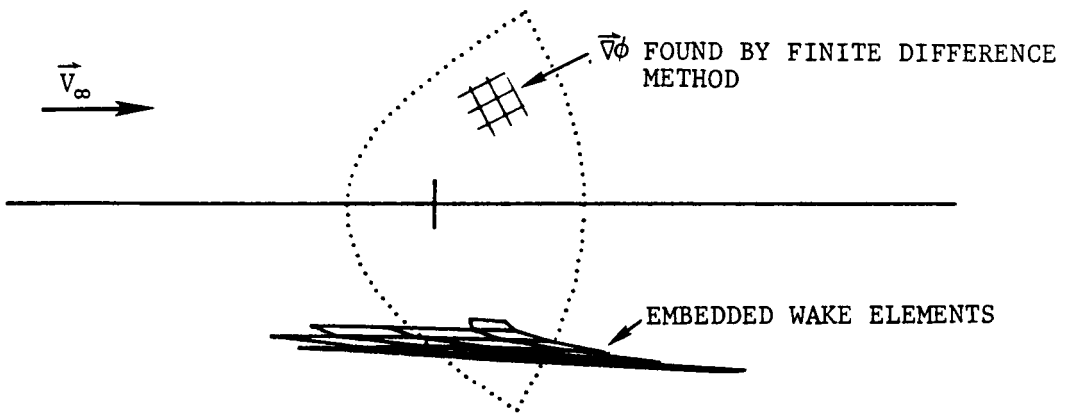

SIDE VIEW

Figure 3b) Embedded Wake Lattice -- From Which Arises the $\vec{V}_1$ Velocity Field

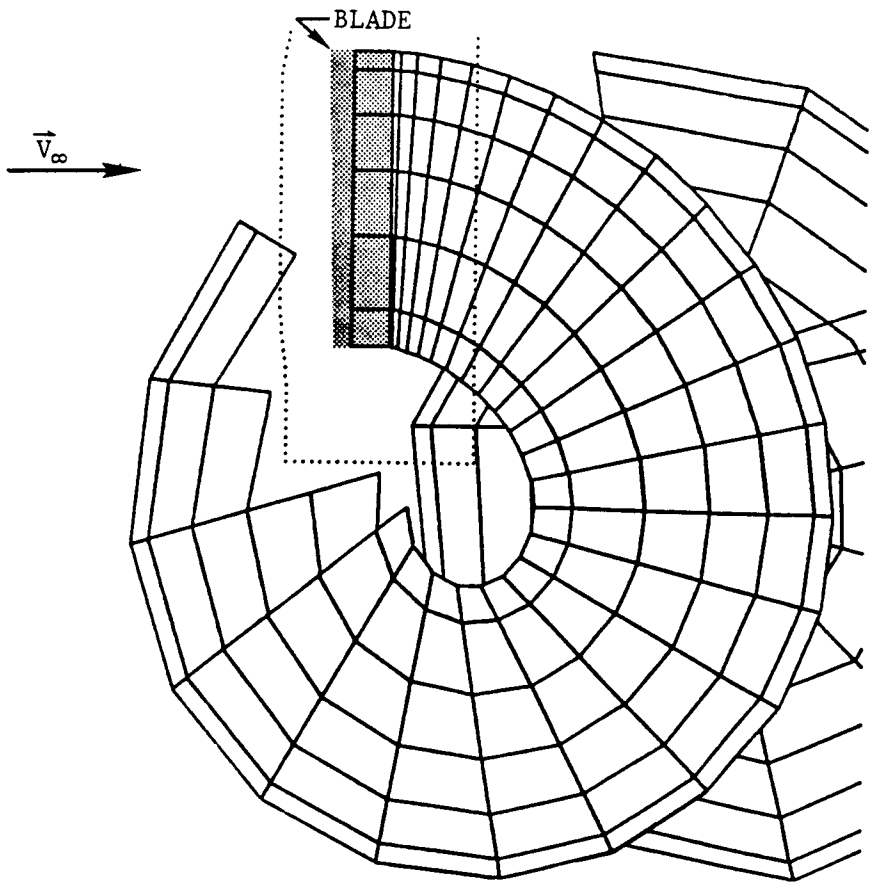

TOP VIEW

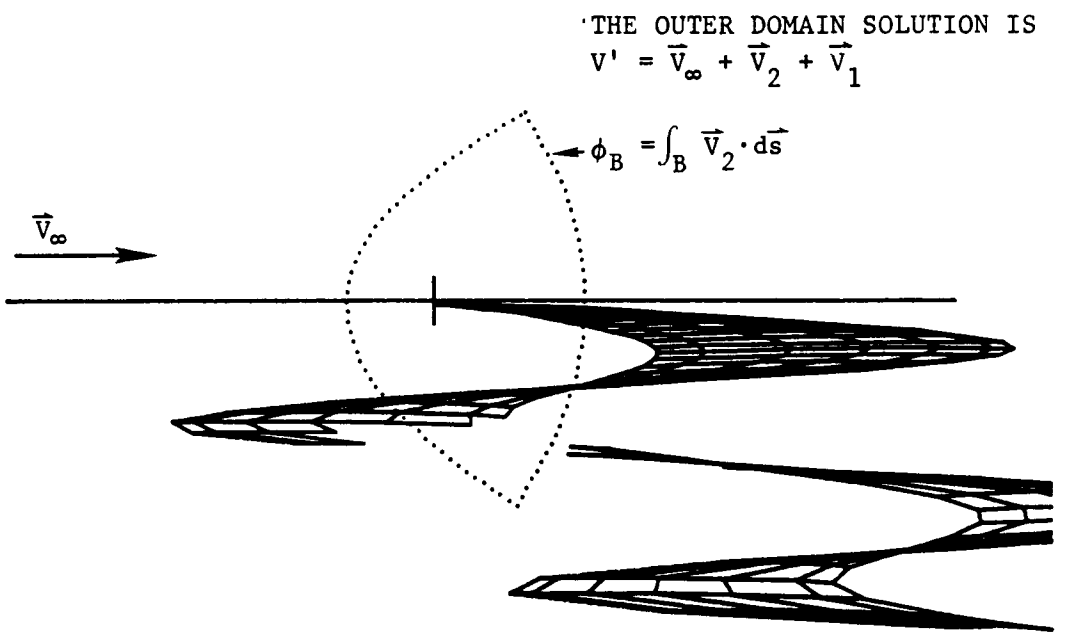

SIDE VIEW

Figure 3c) Wake Lattices External to the Inner Domain -- From Which Arises the $\vec{V}_2$ Velocity Field

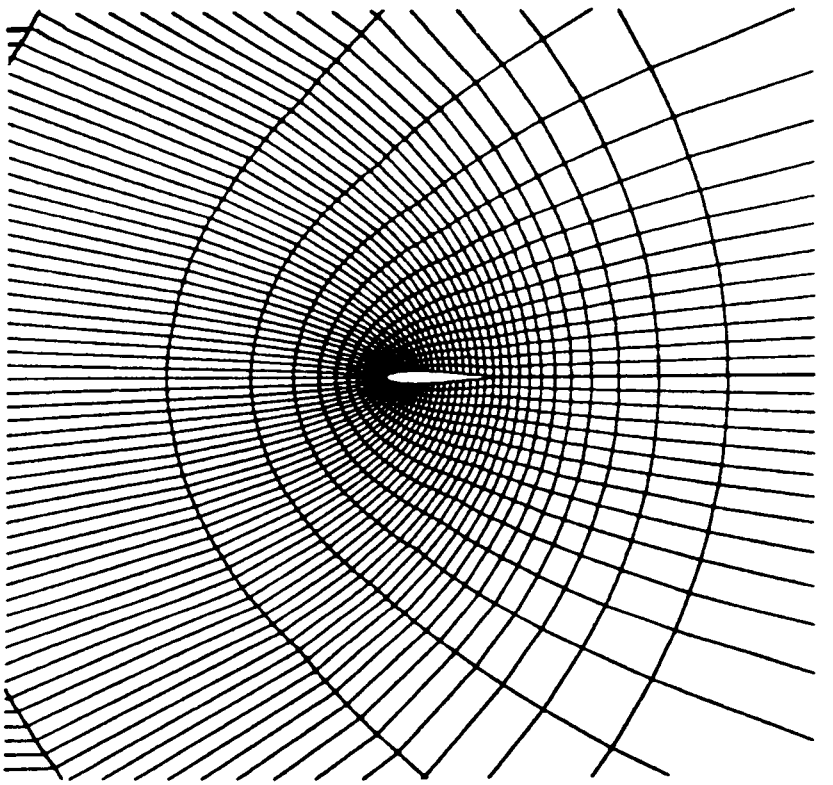

INFINITE DOMAIN

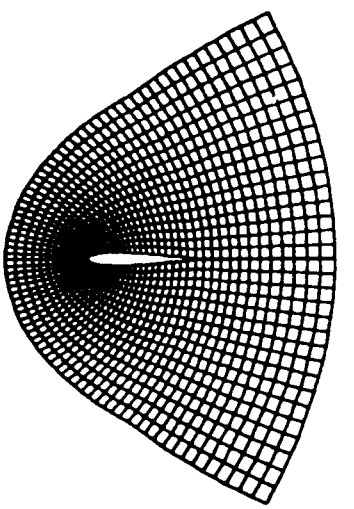

FINITE DOMAIN

Figure 4 Infinite Domain and Finite Domain

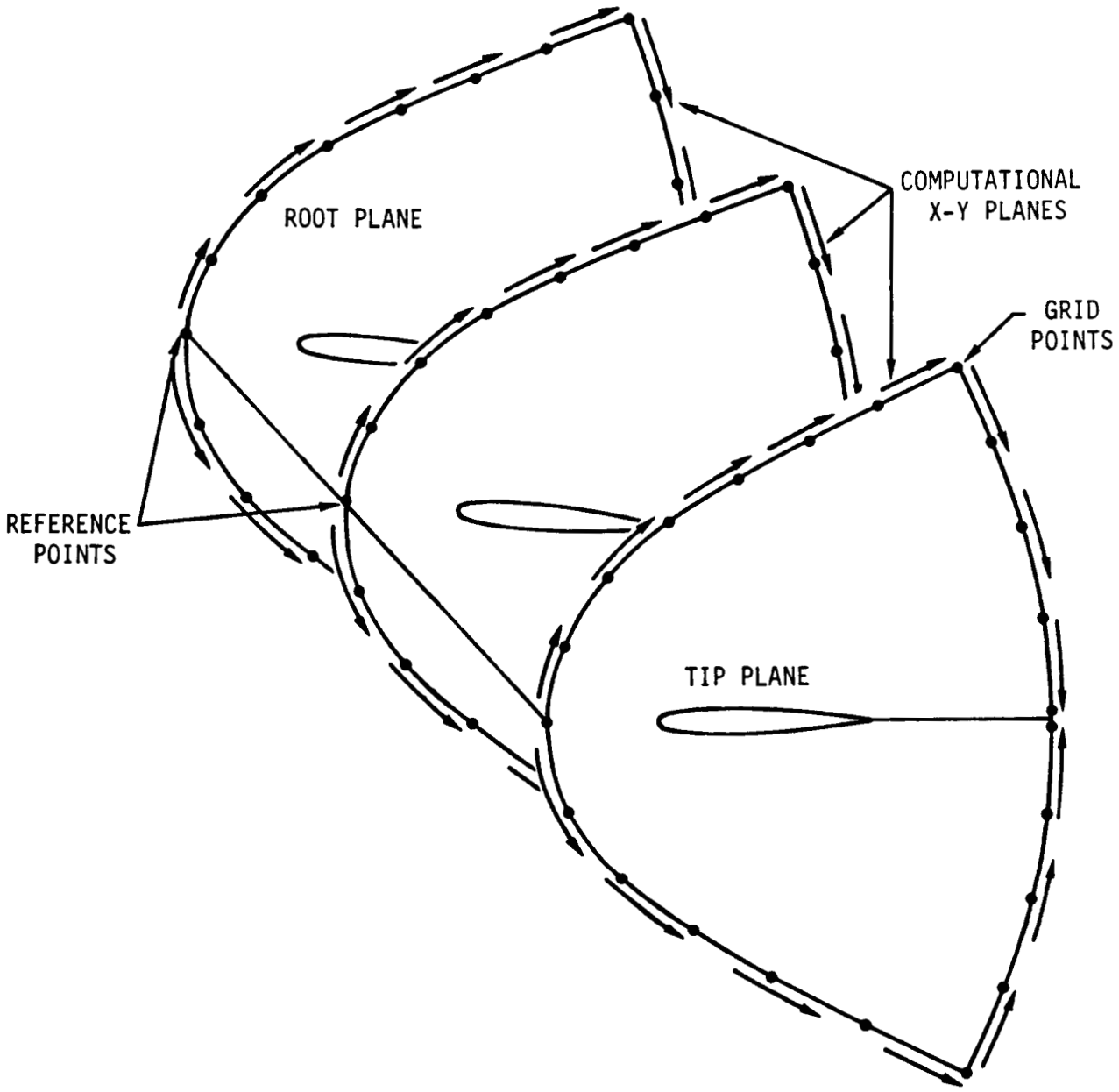

Figure 5 Schematic of Integration Paths on Outer Surface of the Domain

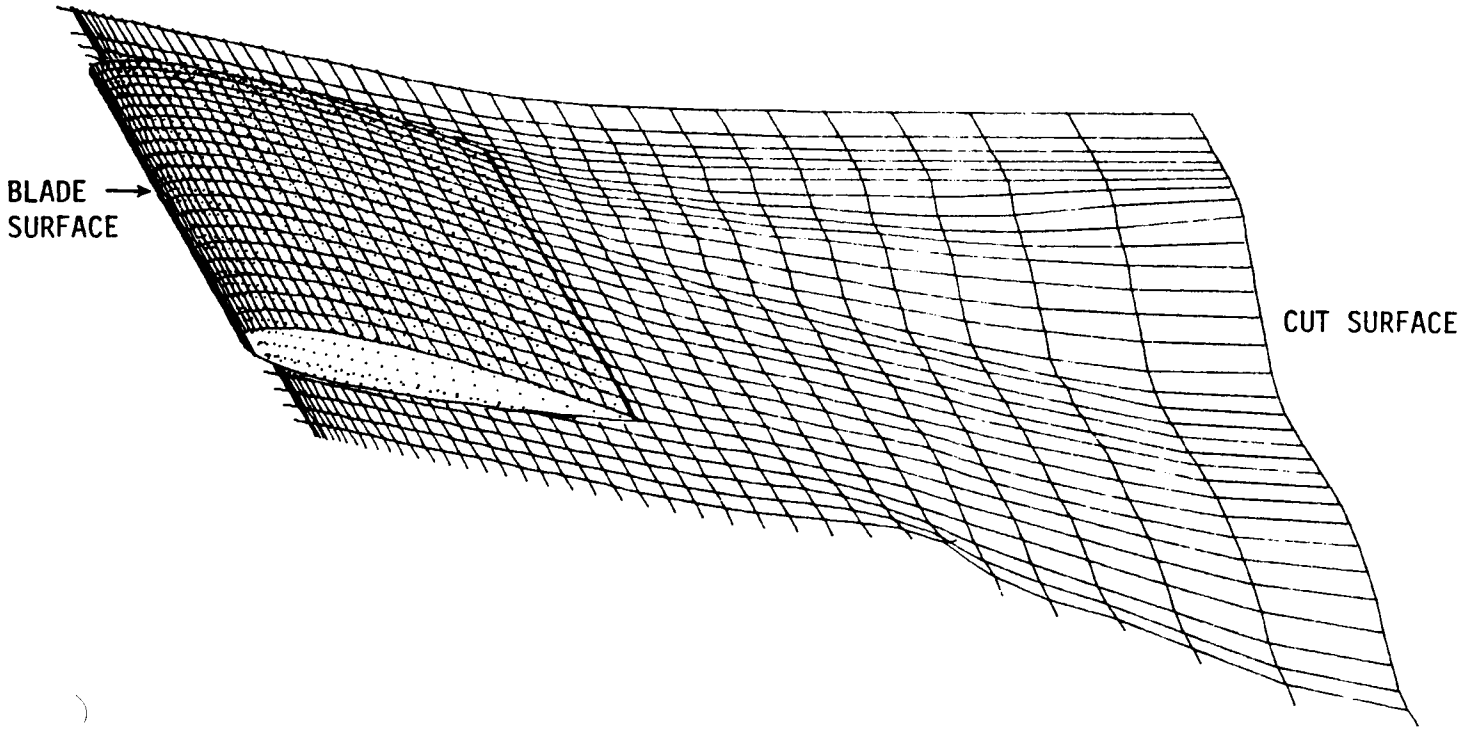

Figure 6 Example of Finite Differance Cut Surface
Mesh Fitted to Prescribed Wake Shape

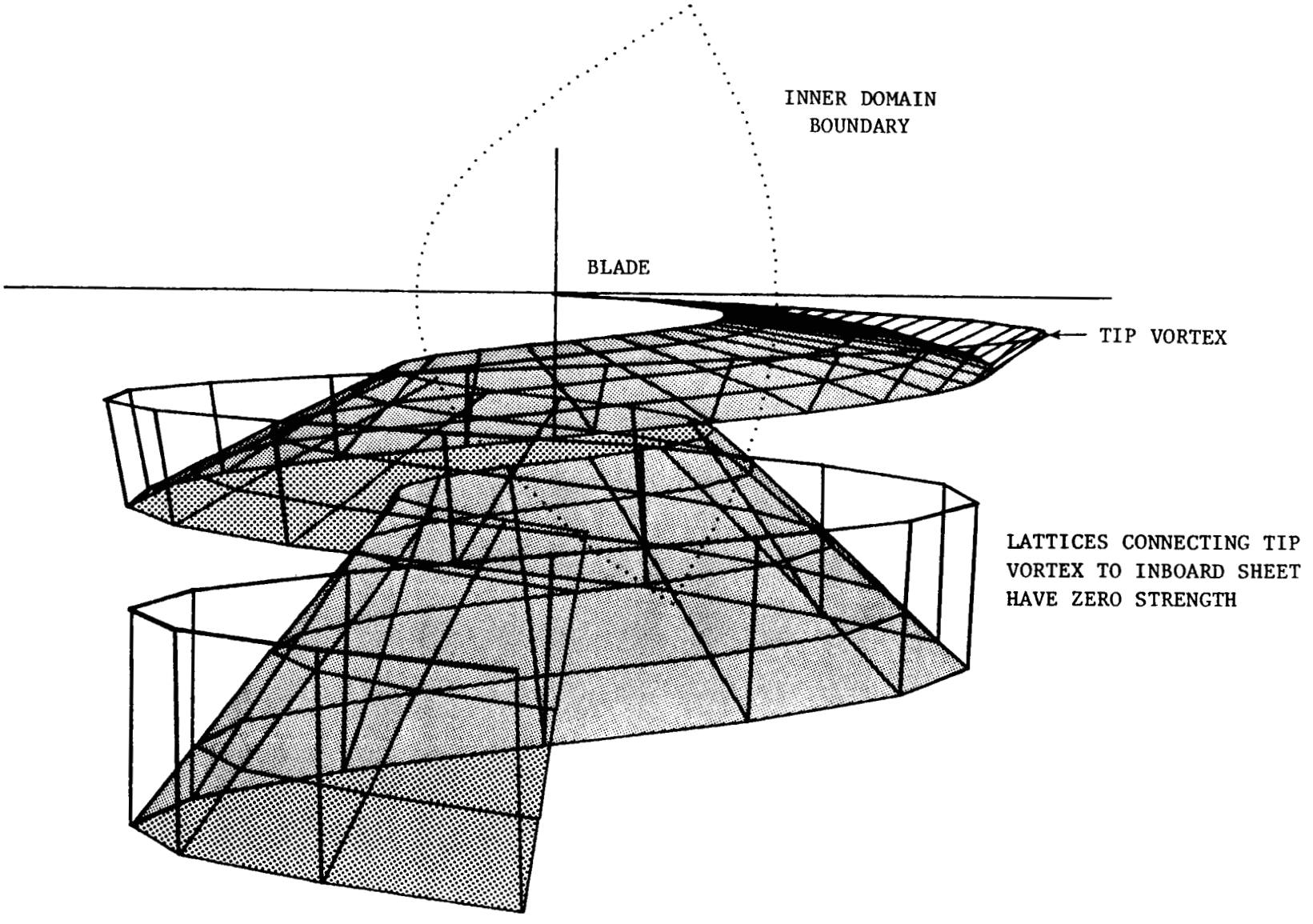

Figure 7 Example Hover Wake Geometry for One Blade

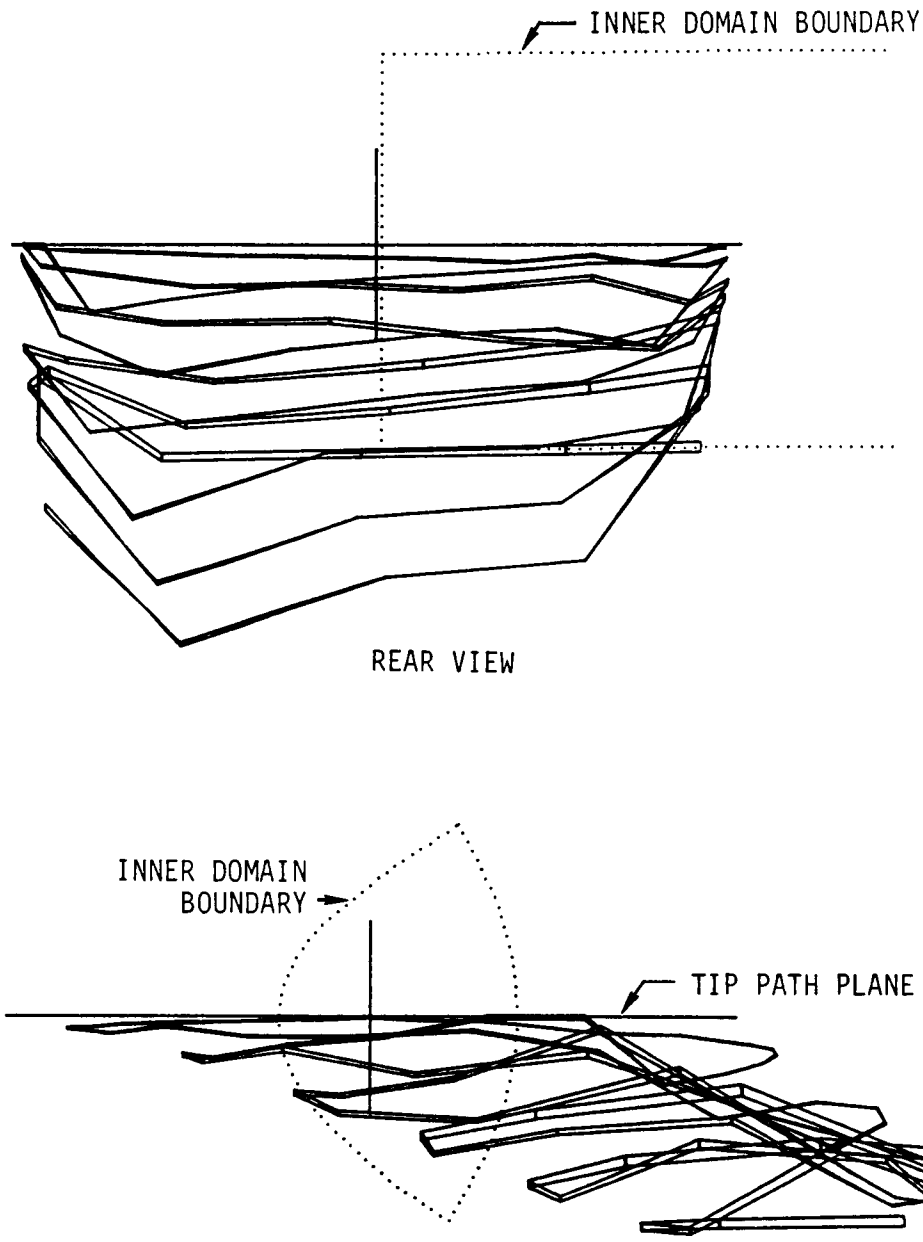

Figure 8 Example of Forward Flight Tip Filament Geometry Based on UTRC Generalization, $\mu = 0.1$.

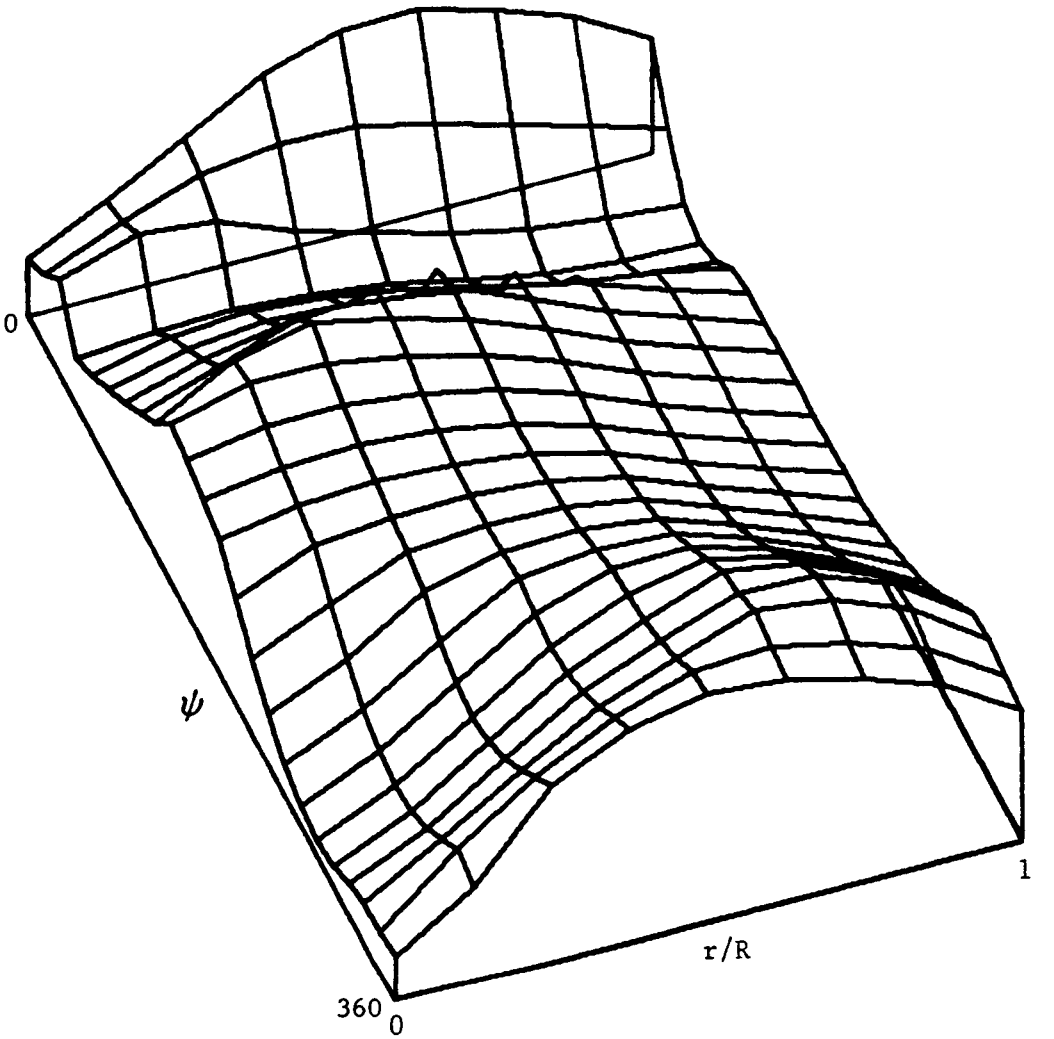

Figure 9 Example of Azimuthal Variation of Blade Bound Circulation as Predicted by F389SR

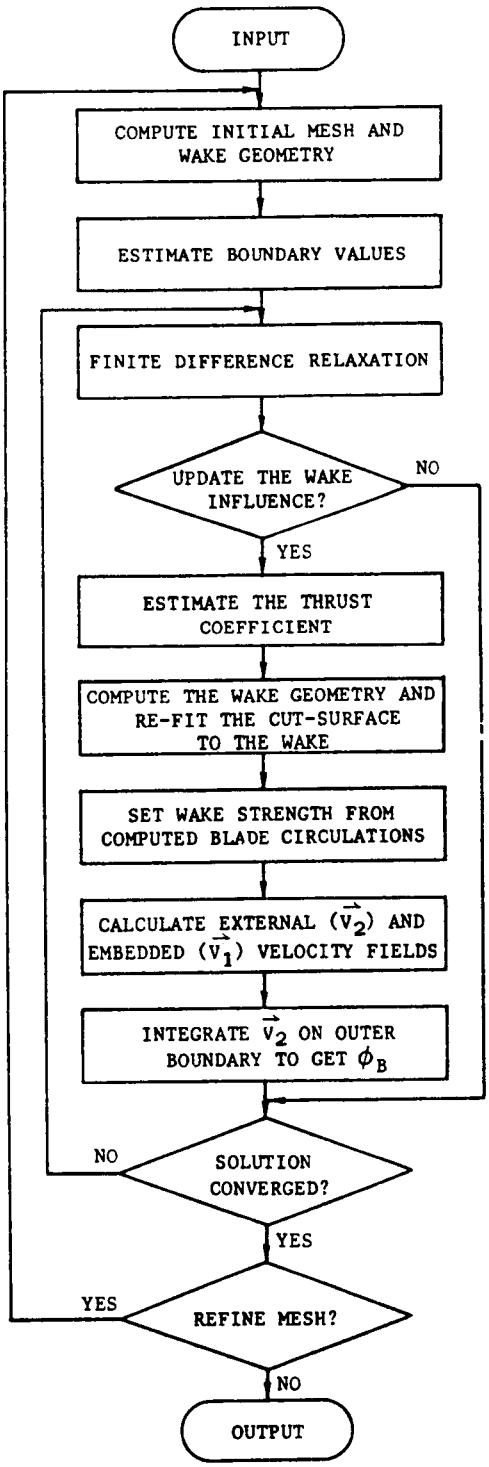

Figure 10 Solution Procedure Flow Chart

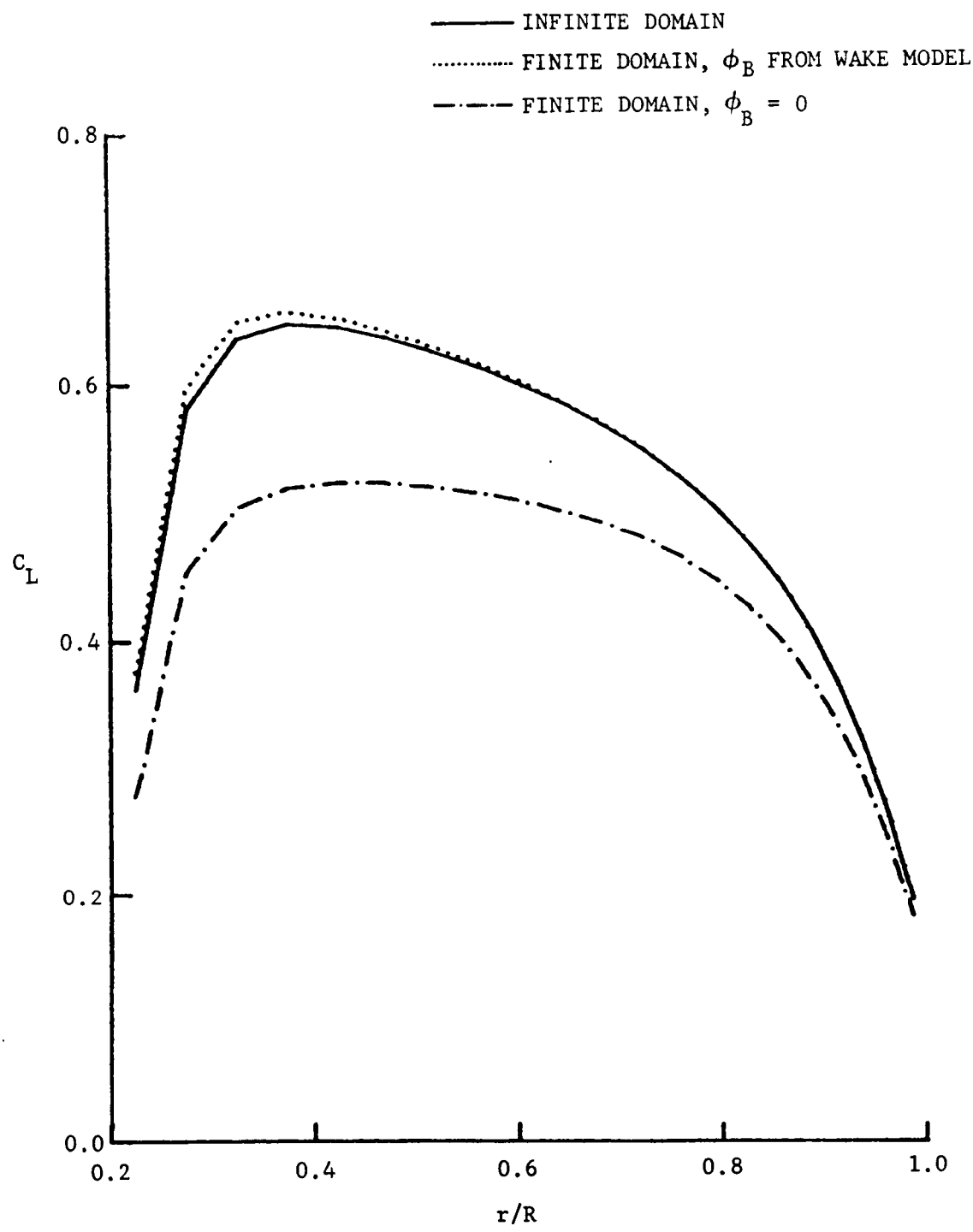

Figure 11 Verification of the Boundary Interaction Concept for Finite Domains, M_∞ = .44

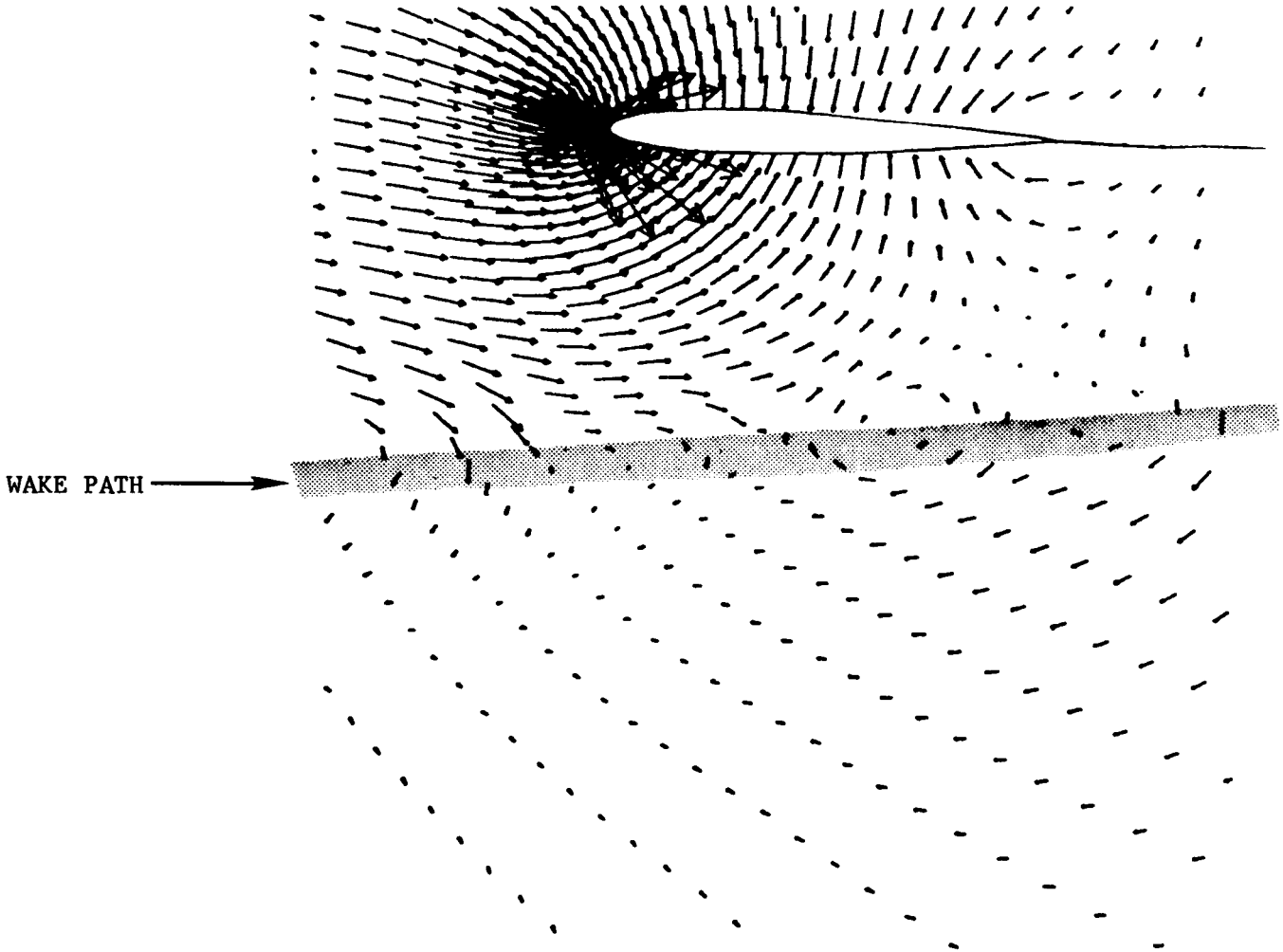

Figure 12 Disturbance Velocity Field Associated with the Embedded Wake

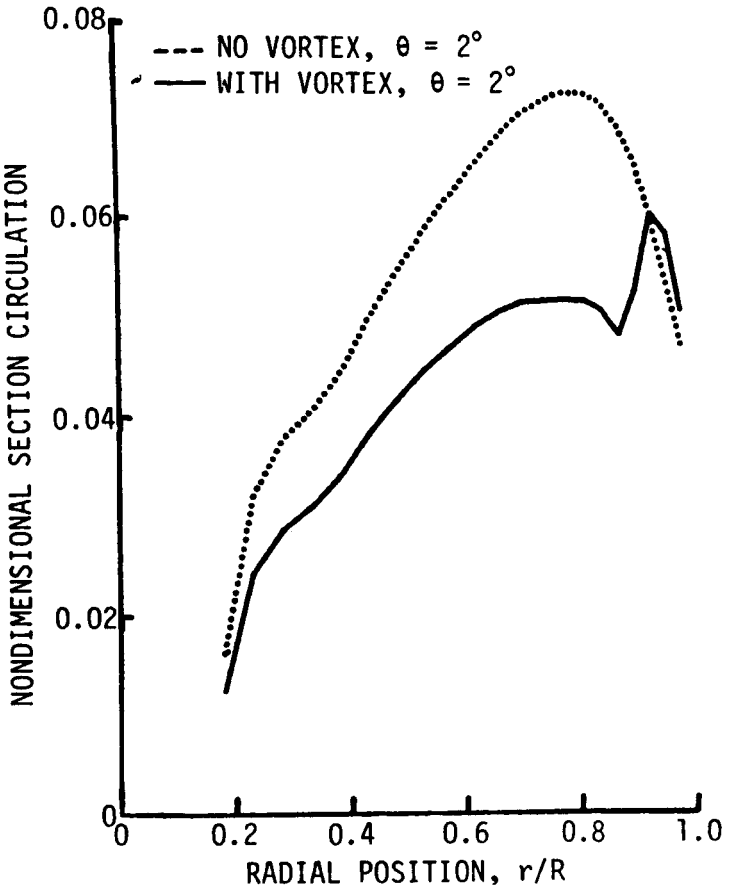

Figure 13(a) Effect of Near Tip Vortex on Hover Airload Solution

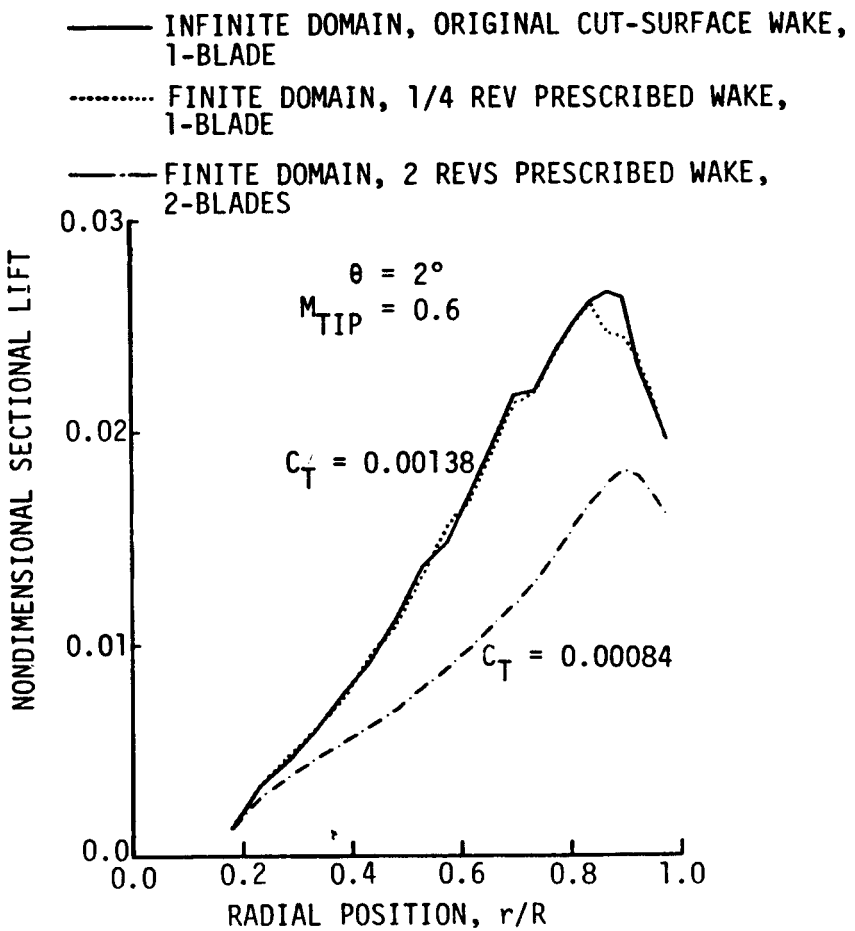

Figure 13(b) Effect of Wake on Hover Airload Solution (Neglecting Near Tip Vortex)

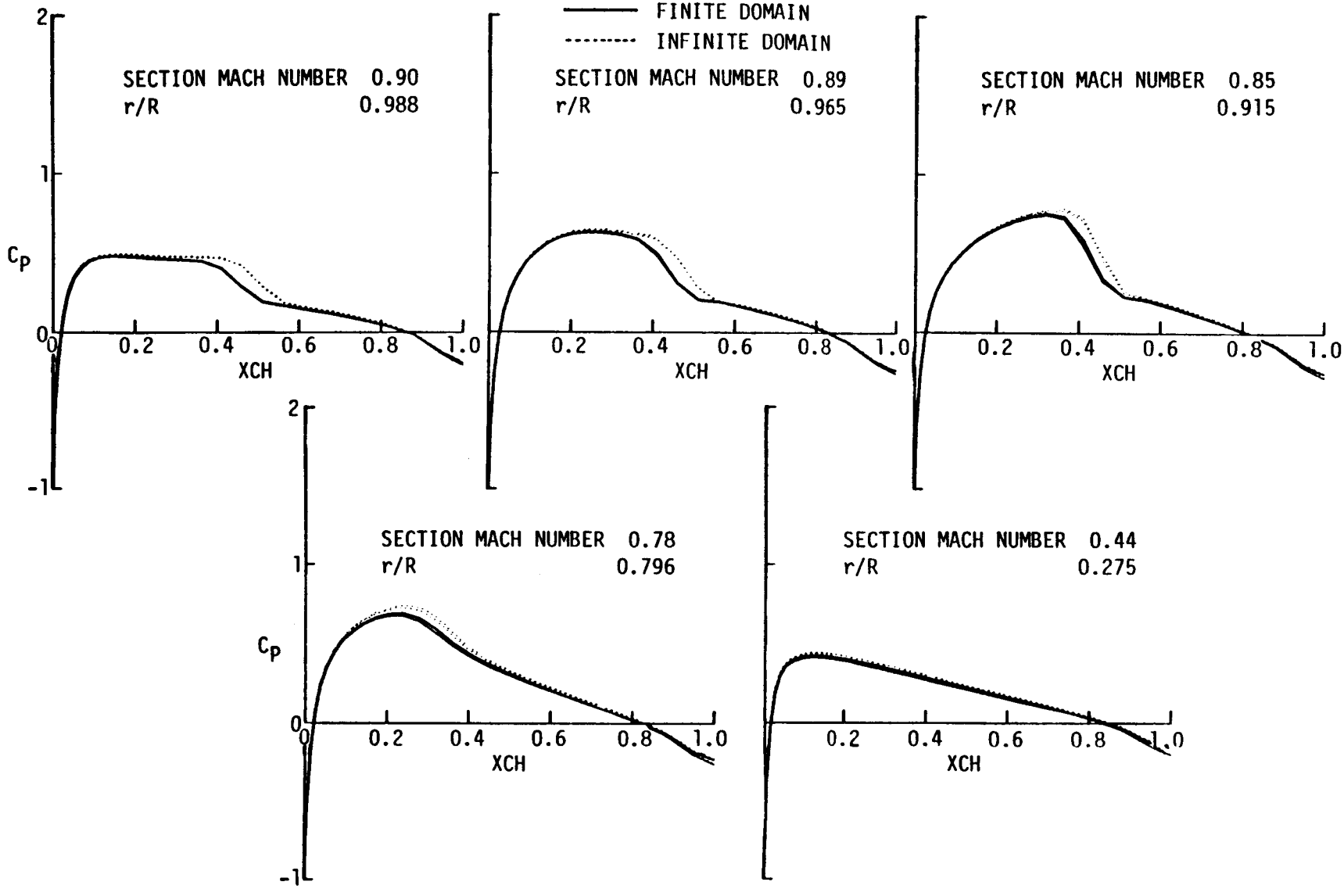

Figure 14 Computed Pressure Distributions at Various Span Stations Showing the Difference Between Infinite Domain and Finite Domain Solutions for a High Tip Speed Non-Lifting Case, NACO012

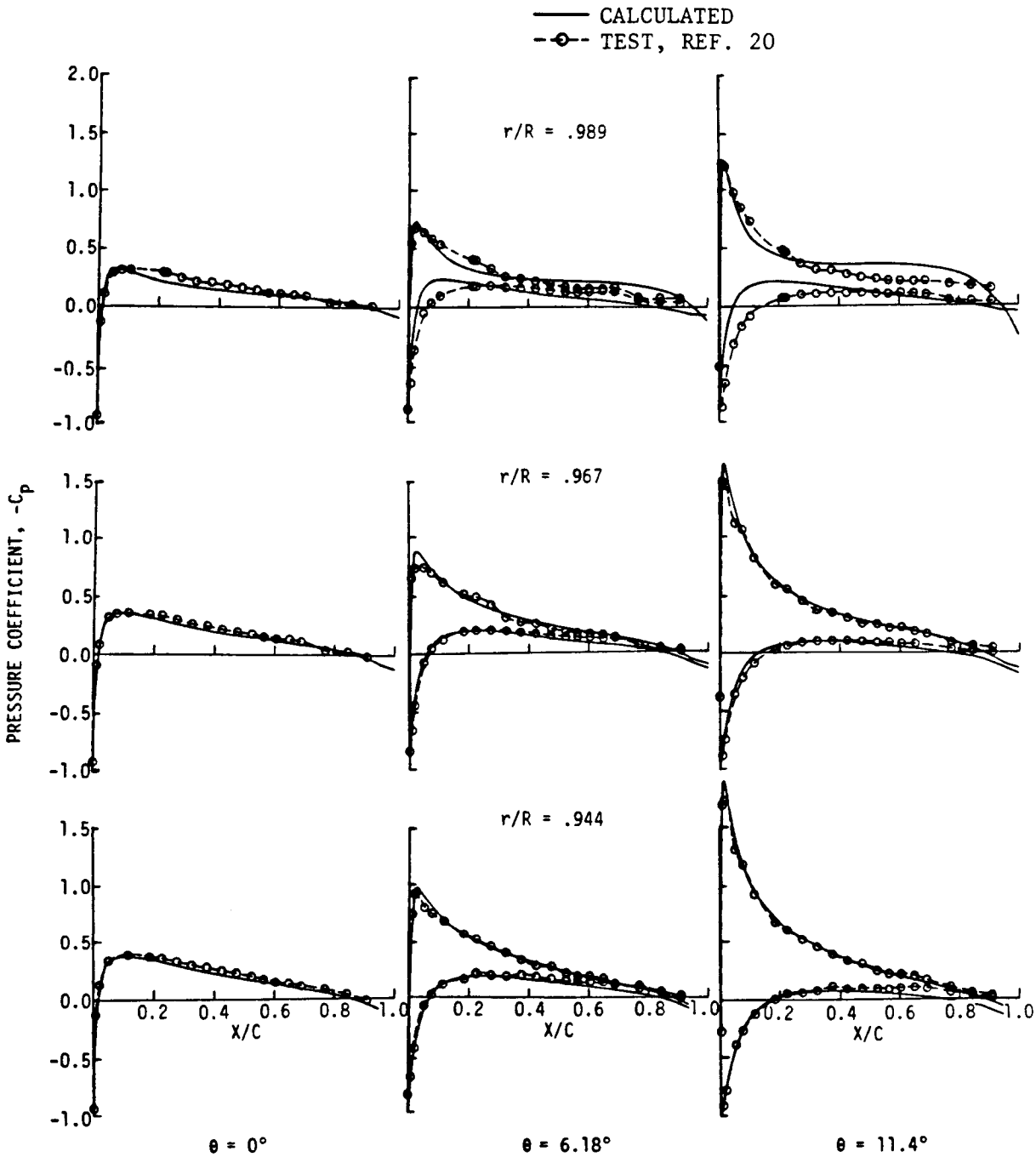

Figure 15 Comparison of Measured and Calculated Pressures for a Single Bladed Rotor at Three Pitch Settings

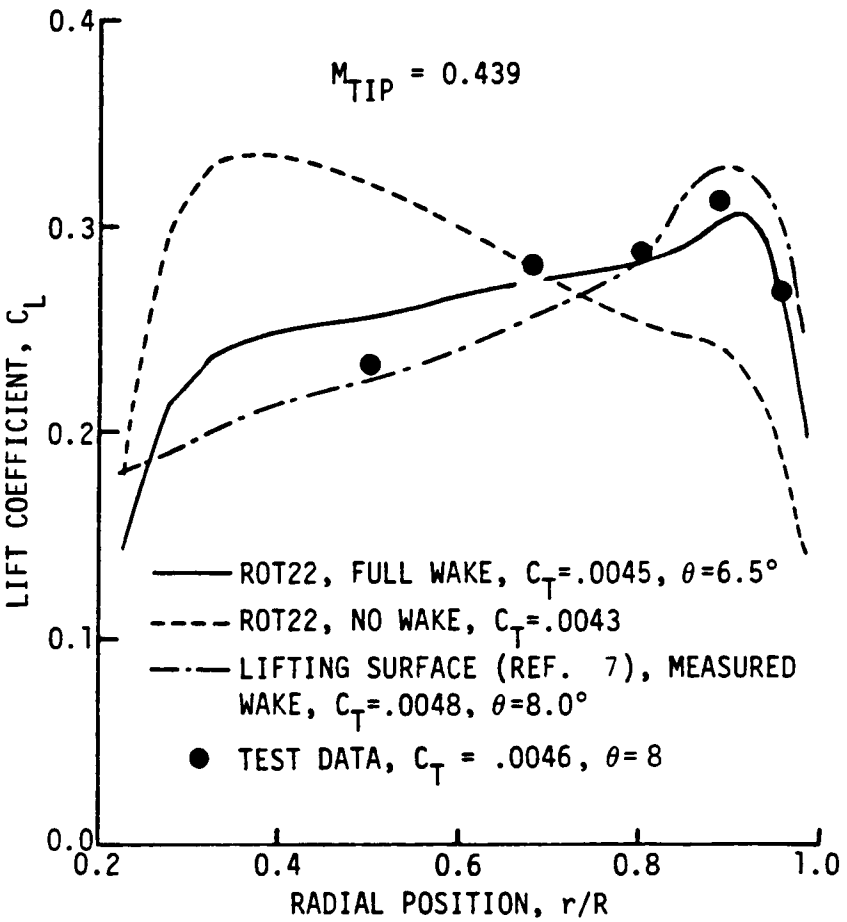

Figure 16 Comparison of Predicted and Measured Spanwise Section Lift Coefficients Reproduced in Part From Ref. 21

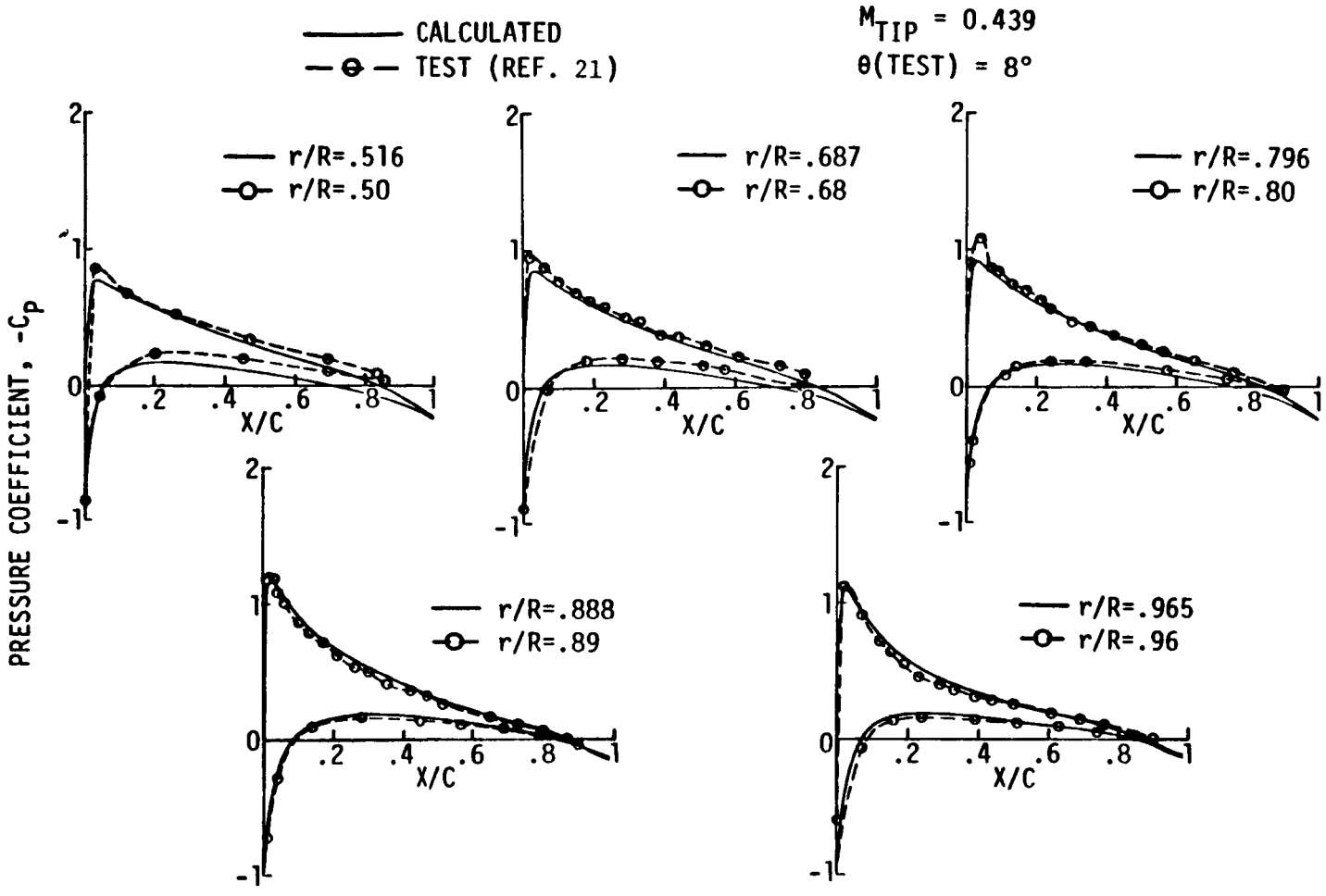

Figure 17 Comparison of Measured and Calculated Pressures at Various Radial Locations for Low Tip Speed

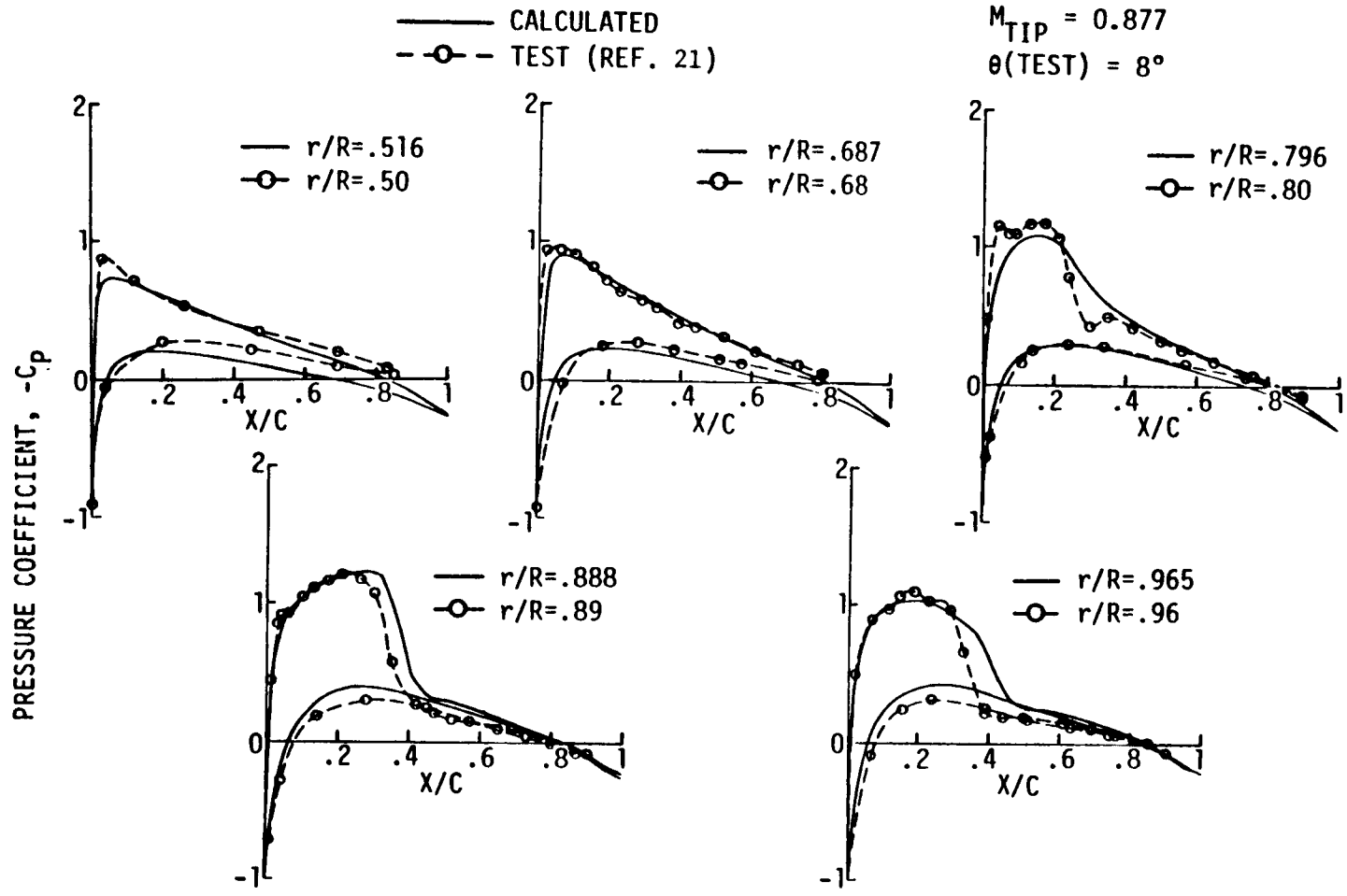

Figure 18 Comparison of Measured and Calculated Pressures at Various Radial Locations for High Tip Speed

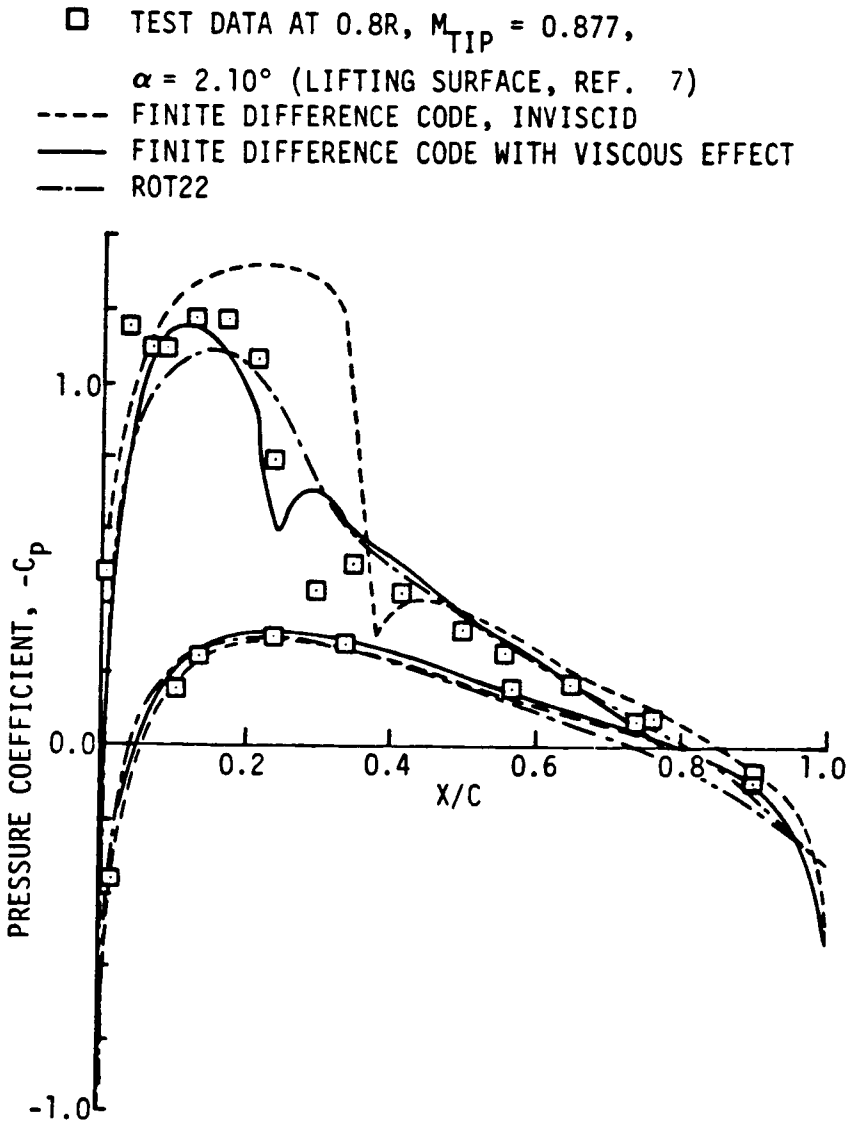

Figure 19 Comparison of Measured and Predicted Chordwise Pressure Distribution at the 0.8R Station, Reproduced in Part From Ref. 21

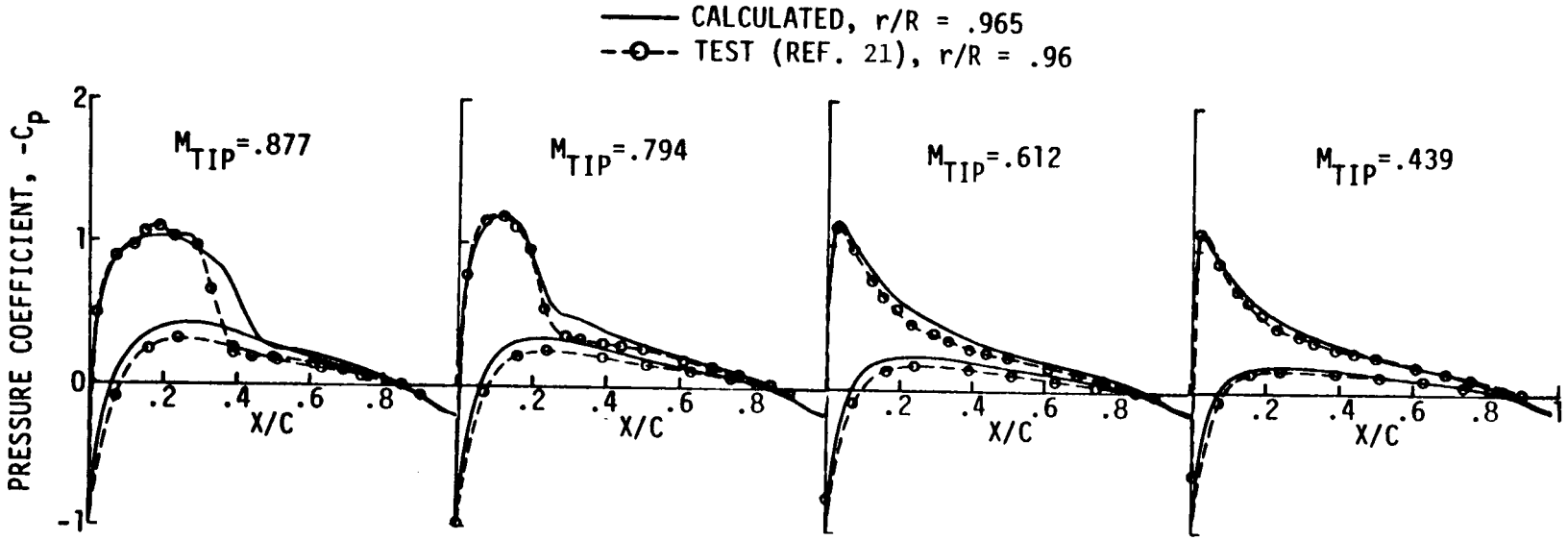

Figure 20 Comparison of Measured and Calculated Pressures for a Range of Tip Mach Numbers

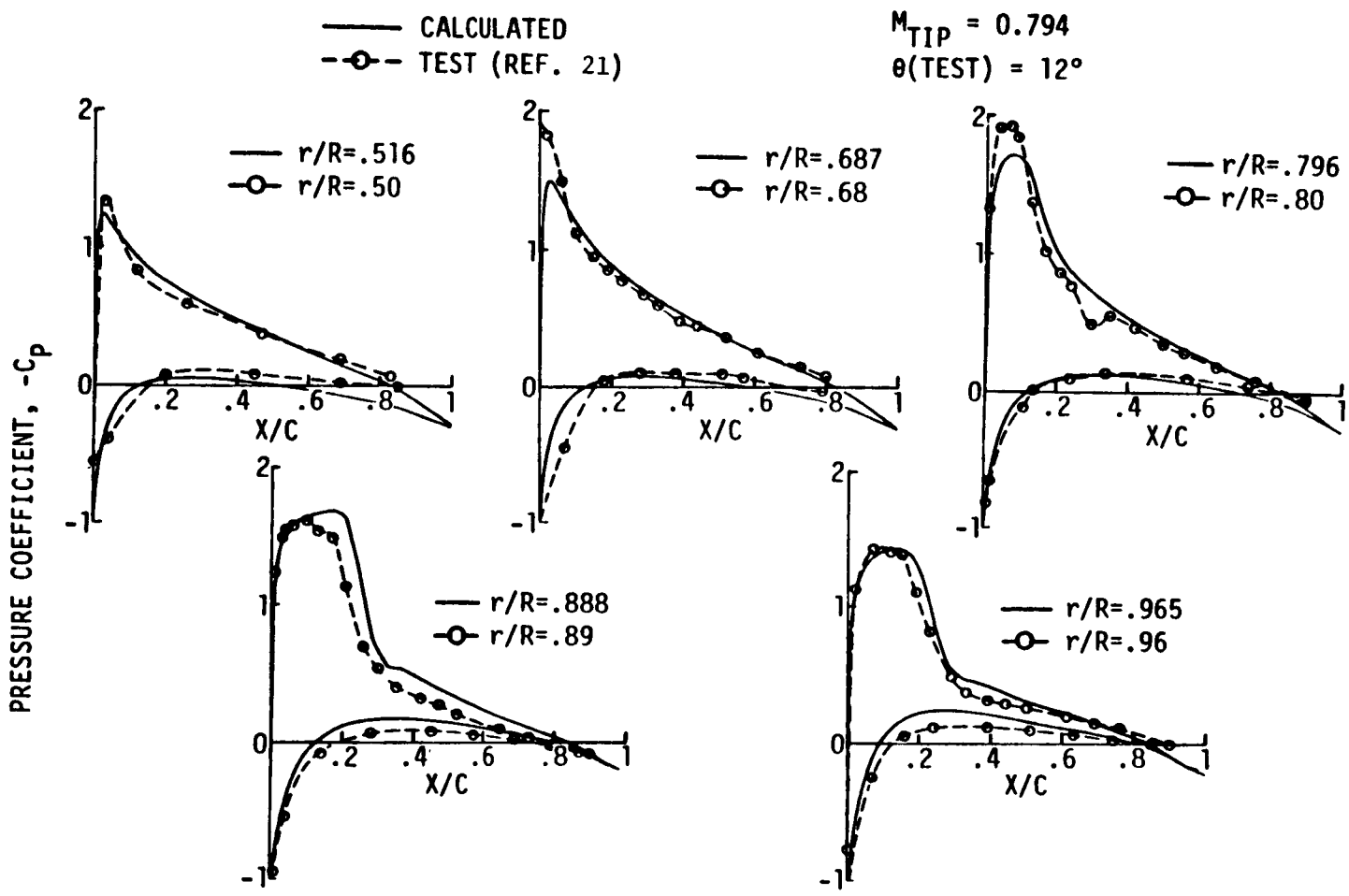

Figure 21 Comparison of Measured and Calculated Pressures for High Tip Speed and High Collective Pitch

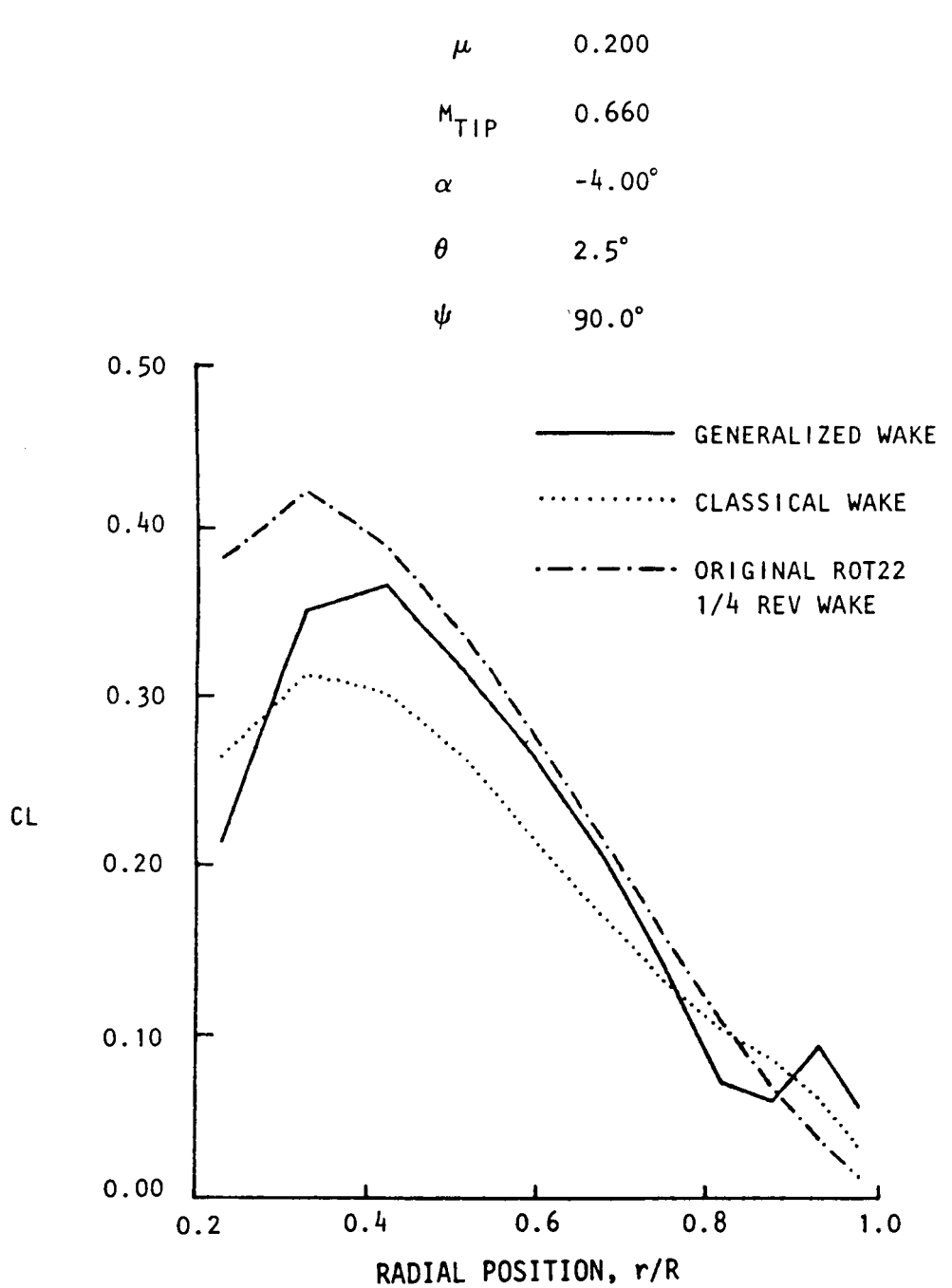

Figure 22 Comparison of Predicted Blade Loadings for Different Wake Models

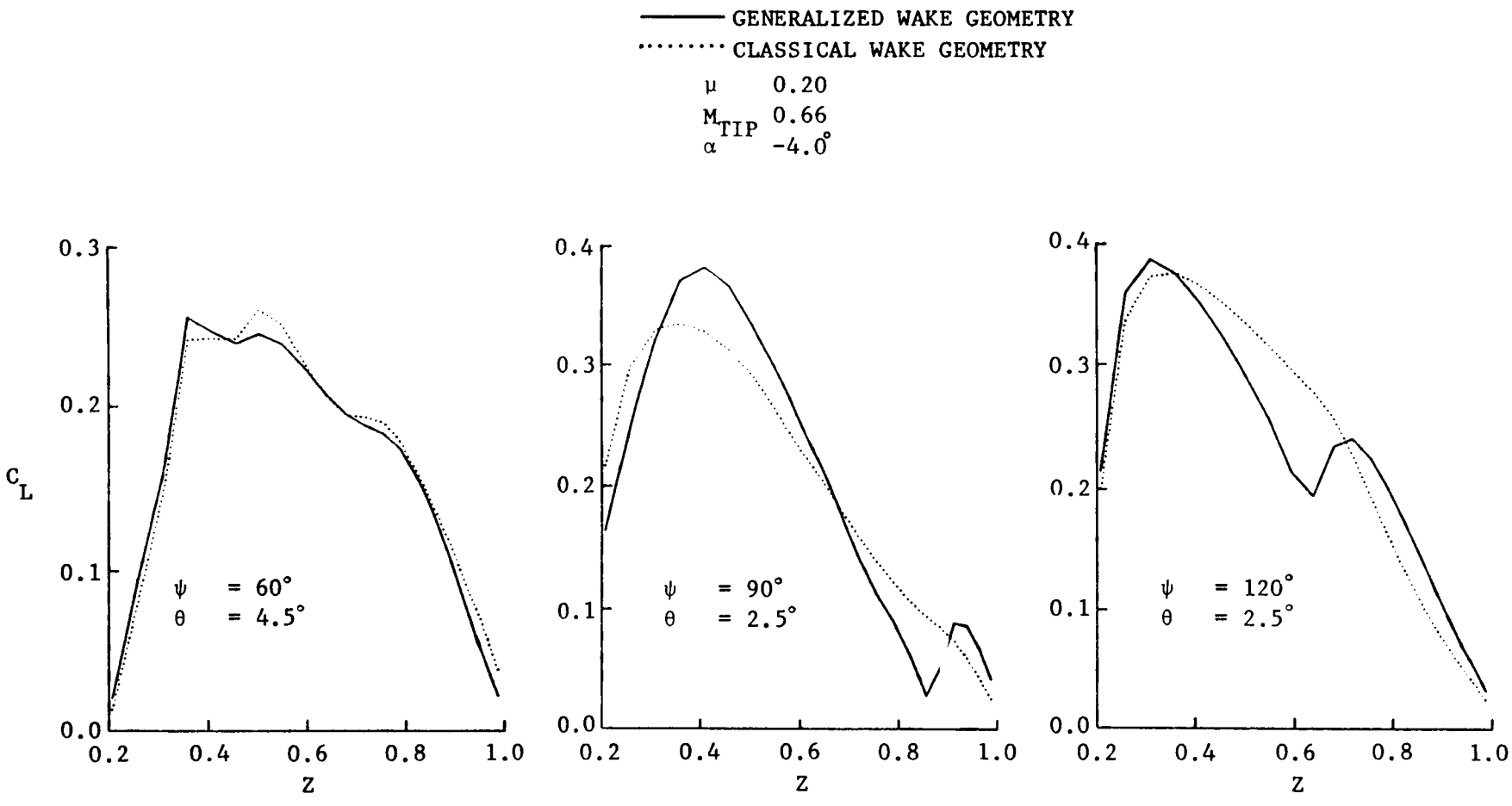

Figure 23 Blade Load Distributions for μ = 0.2

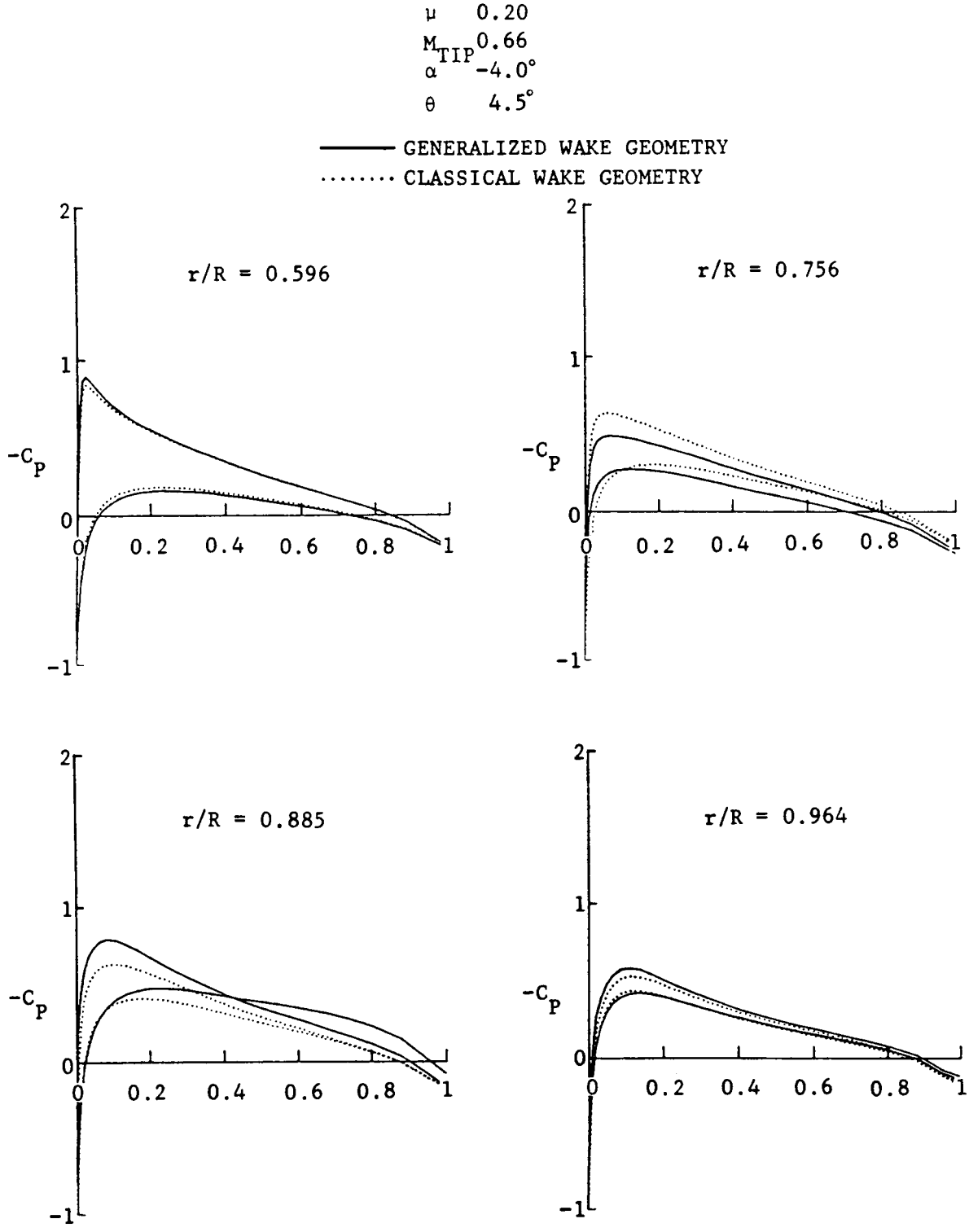

Figure 24 Blade Surface Chordwise Pressure Distributions for $\mu = 0.20$, $\psi = 90^\circ$

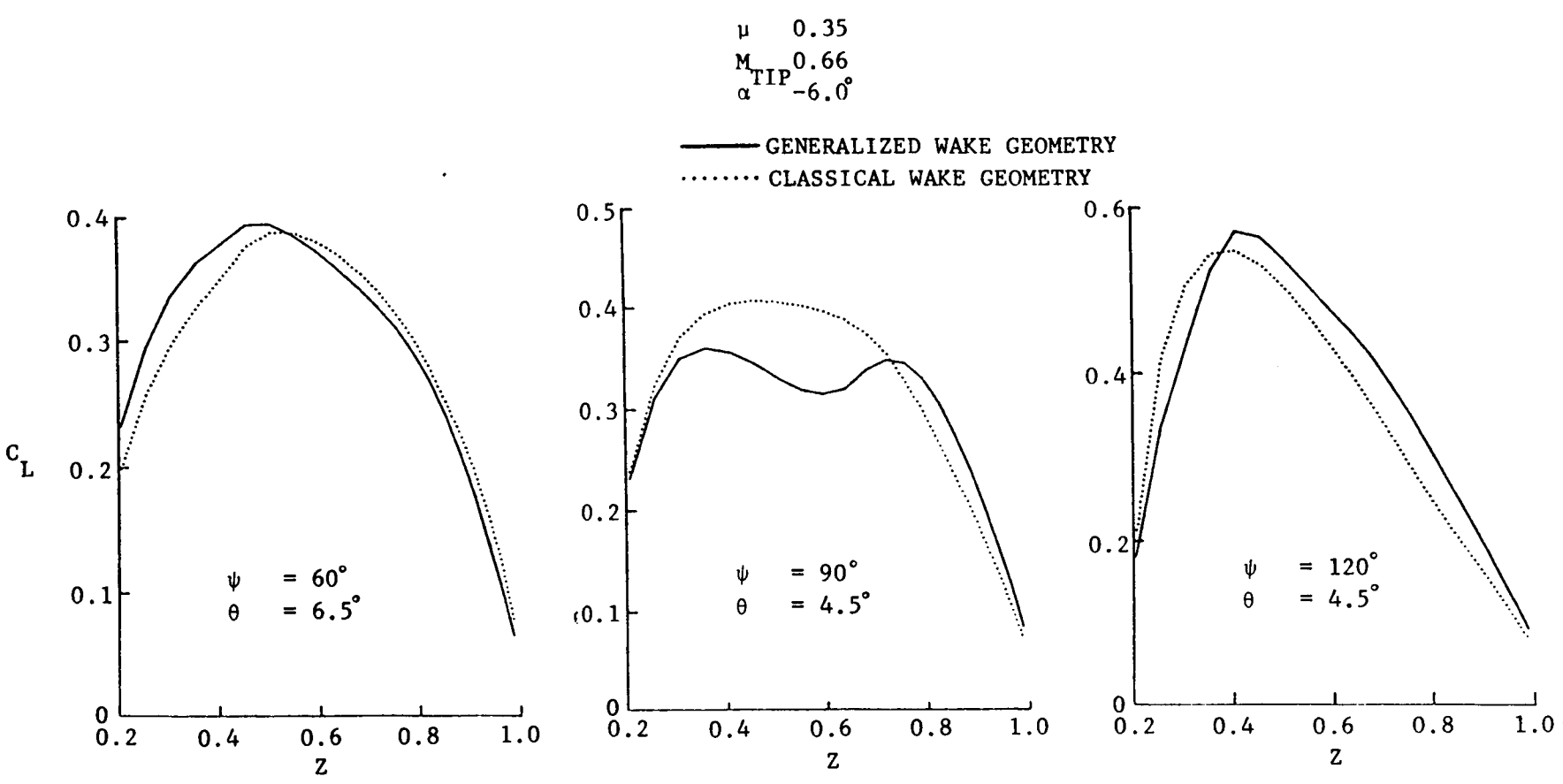

Figure 25 Effect of Wake Models on Load Distributions, μ = 0.35

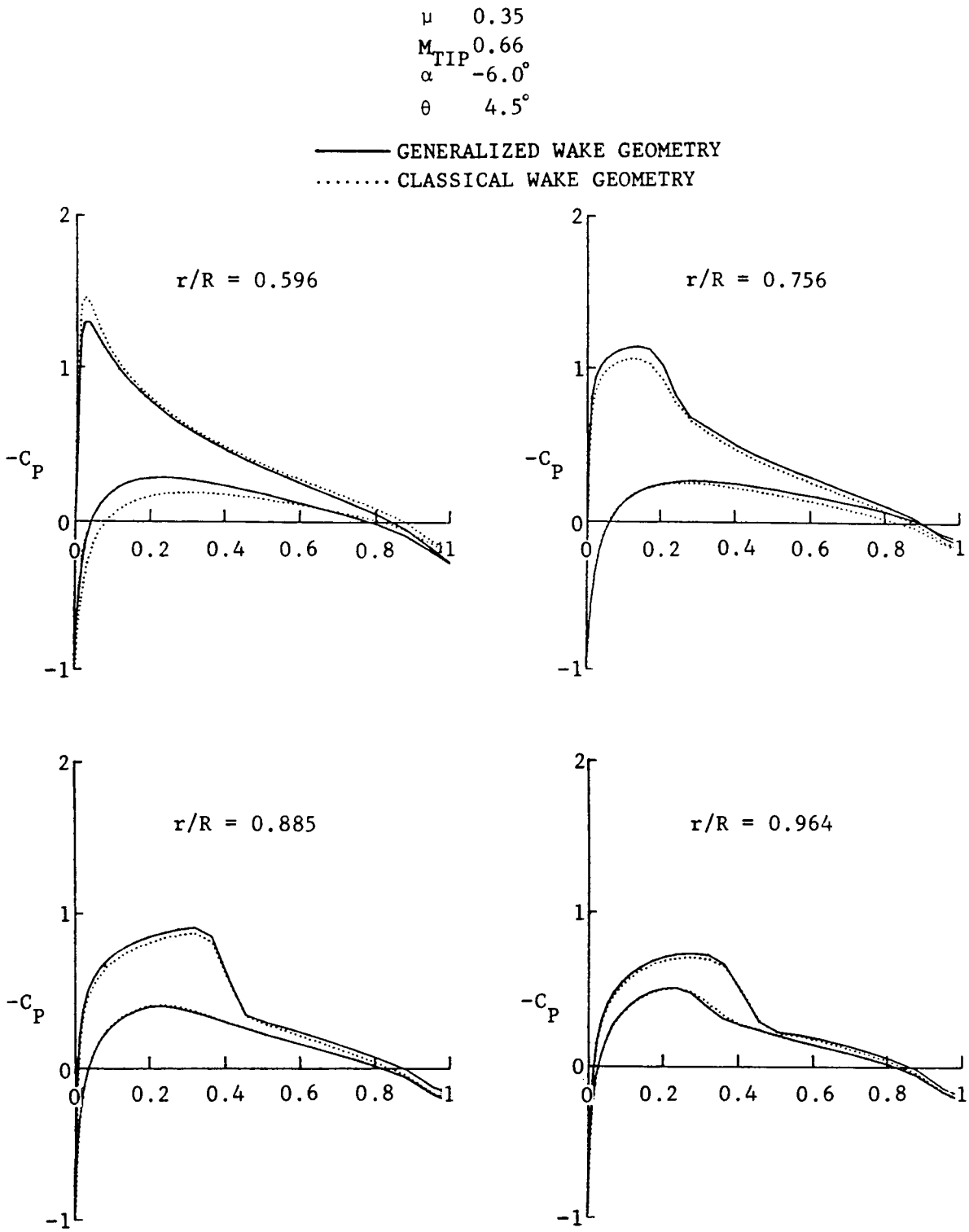

Figure 26 Blade Surface Chordwise Pressure Distributions for $\mu = 0.35$, $\psi = 90°$

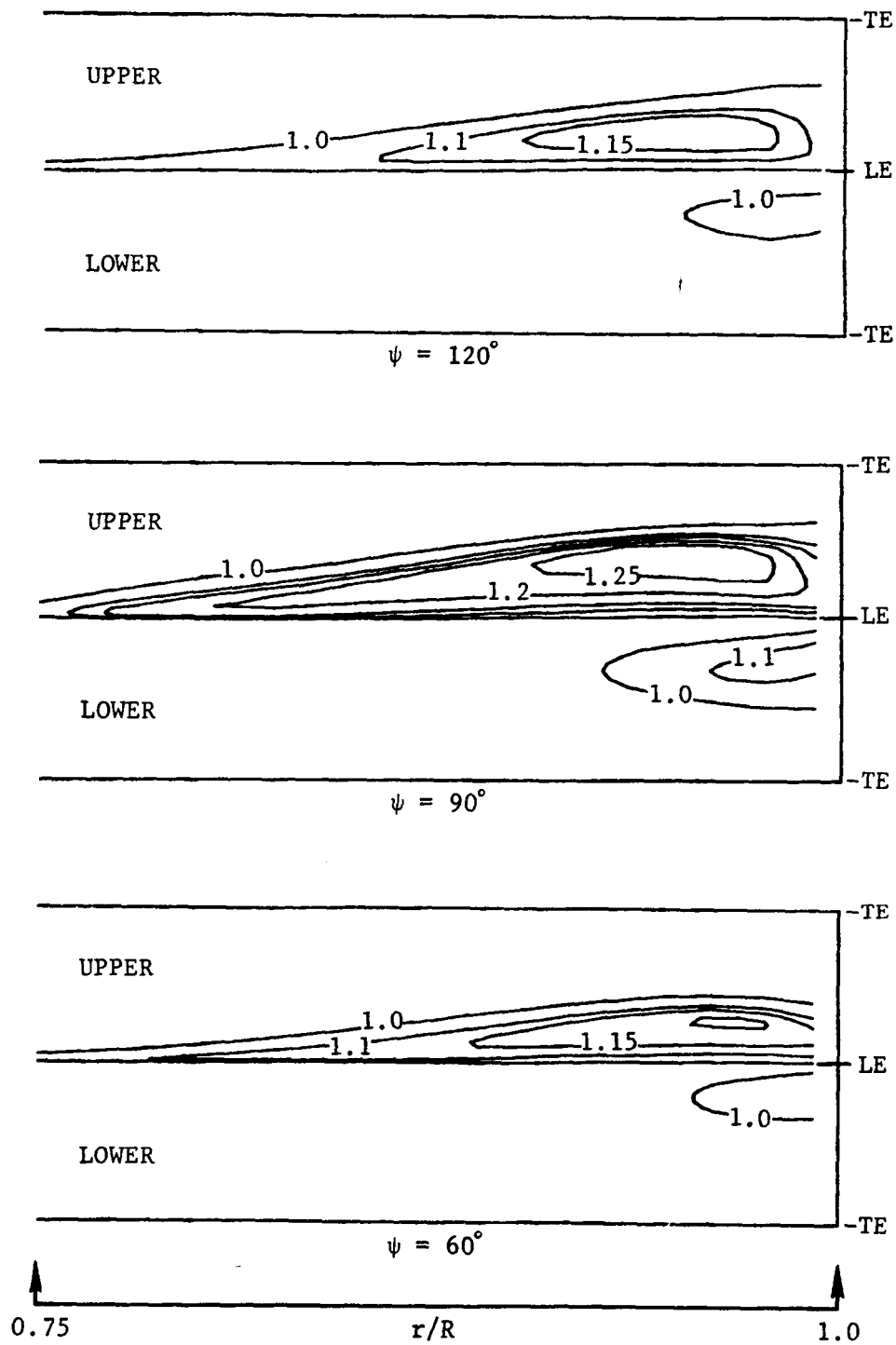

Figure 27 Computed Blade-Surface Mach Contours, $\mu = 0.35$, Generalized Wake

1. Report No.	2. Government Accession No.	3. Recipient's Catalog No.
NASA CR-4007		

4. Title and Subtitle	5. Report Date
A Full Potential Flow Analysis With Realistic Wake Influence for Helicopter Rotor Airload Prediction	January 1987
	6. Performing Organization Code

7. Author(s)	8. Performing Organization Report No.
T. Alan Egolf and S. Patrick Sparks	R86-915999-13
	10. Work Unit No.

9. Performing Organization Name and Address	11. Contract or Grant No.
United Technologies Research Center East Hartford, Connecticut 06108	NAS2-11150
	13. Type of Report and Period Covered
12. Sponsoring Agency Name and Address	Contractor Report
National Aeronautics and Space Administration Washington, DC 20546	14. Sponsoring Agency Code 505-42-11

15. Supplementary Notes

Point of Contact: Michael Tauber, NASA Ames Research Center, ms 229-4, Moffett Field, CA. 94035, FTS 464-6086 or 415-694-6086

16. Abstract

A three-dimensional, quasi-steady, full potential flow solver was adapted to include realistic wake influence for the aerodynamic analysis of helicopter rotors. The method is based on a finite difference solution of the full potential equation, using an inner and outer domain procedure for the blade flowfield to accommodate wake effects. The nonlinear flow is computed in the inner domain region using a finite difference solution method. The wake is modeled by a vortex lattice using prescribed geometry techniques to allow for the inclusion of realistic rotor wakes. The key feature of the analysis is that vortices contained within the finite difference mesh (inner domain) was treated with a vortex embedding technique while the influence of the remaining portion of the wake (in the outer domain) is impressed as a boundary condition on the outer surface of the finite difference mesh. The solution procedure couples the wake influence with the inner domain solution in a consistent and efficient solution process. The method has been applied to both hover and forward flight conditions. Correlation with subsonic and transonic hover airload data is shown which demonstrates the merits of the approach.

17. Key Words (Suggested by Author(s))	18. Distribution Statement
Rotor, Helicopter, Full Potential, Rotor Wake, Airloads, Embedded Vortex, Inner/Outer Domain, Rotor Aerodynamics	Unclassified - Unlimited Subject Category 01

19. Security Classif. (of this report)	20. Security Classif. (of this page)	21. No. of Pages	22. Price
Unclassified	Unclassified	74	A04

For sale by the National Technical Information Service, Springfield, Virginia 22161

NASA-Langley, 1987